International Journal of Solids and Structures 49 (2012) 3774–3796

Contents lists available at SciVerse ScienceDirect

International Journal of Solids and Structures

journal homepage: www.elsevier.com/locate/ijsolstr

Contact variables and thermal effects at the tool–chip interface in orthogonal cutting

A. Molinari [a,b,*], R. Cheriguene [a,b], H. Miguelez [b]

[a] Laboratoire d'Etude des Microstuctures et de Mécanique des Matériaux, LEM3, CNRS, Université de Lorraine, Ile du Saulcy, 57045 Metz, France
[b] Department of Mechanical Engineering, Carlos III University – Madrid, Calle Butarque 15, 28911 Leganes, Madrid, Spain

ARTICLE INFO

Article history:
Received 23 June 2011
Received in revised form 4 July 2012
Available online 24 August 2012

Keywords:
Orthogonal cutting
Friction
Sticking contact
Interface heating
Boundary layer

ABSTRACT

This paper is aimed at providing a comprehensive analysis of the contact problem in orthogonal cutting based on the simple assumption that contact is governed by a Coulomb law. Effects of the sliding friction coefficient and of the cutting conditions are analyzed in details. The problem is analyzed numerically by using an Arbitrary Lagrangian Eulerian Finite Element technique. In parallel, analytical models are developed allowing us to interpret the numerical data and to make them more meaningful. Distributions along the tool–chip interface are analyzed for stresses, temperature and sliding velocities. The shear stress exerted along the sticking zone is found to be equal to the shear flow stress of the work-material. Of particular significance is the investigation of the interface heating as the chip temperature appears to be a key factor governing the contact regime. The increasing of the chip temperature along the tool rake face appears to be mainly controlled by the mean value of the shear stress on the rake face and the Péclet number taking into account the phenomena of advection and heat diffusion. At low values of the friction coefficient the contact is governed by chip–tool sliding for the whole range of cutting speeds considered here ($1\ ms^{-1} \leqslant V \leqslant 50\ ms^{-1}$). For larger values of the sliding friction coefficient, a transition to a contact dominated by sticking is found when the cutting speed is increased. Then, contact variables appear to be mostly determined by the value of the flow stress of the work-material with a negligible effect of the sliding friction coefficient. Thermal softening of the flow stress of the work-material governs the relationship between cutting variables and cutting conditions. An asymptotic regime occurs at relatively high cutting velocities (larger than 10 m/s) and for values of the sliding friction coefficient larger than 0.4. The analysis of the effects of cutting conditions on the morphology of the secondary shear zone reveals the existence of a boundary layer regime in the range of high cutting velocities. This is in keeping with the occurrence of the asymptotic regime mentioned above.

Despite the simplicity of the contact model used, reasonable agreement is obtained with respect to experimental trends. The interplay between numerical and analytical approaches happens to be fruitful for understanding which are the main parameters influencing the contact variables, for checking the consistency of the numerical approach and for offering a route for future improvements of machining models.

1. Introduction

The modeling of cutting processes appears to be a challenging task since complex interactions between a number of parameters are involved. Moreover, material parameters and interface properties are difficult to characterize. The constitutive law of the work-material has to be determined under the extreme conditions met during machining (large deformations, high temperatures and high strain rates). The physical mechanisms controlling friction in dry cutting are insufficiently known. This is especially the case at high cutting speeds. Considering for instance high speed cutting of steels, the order of magnitude of physical parameters at the tool–chip interface is about 10 m/s for the sliding velocity, 1 GPa for the normal stress and 1300 K for the temperature.

The tool–chip contact is analyzed in this paper. How process variables are affected by friction characteristics is of particular interest. Dry cutting conditions are assumed. The evolution of local variables at the tool–chip interface (stresses, particle velocities, temperature) with cutting conditions is described in details. This work is mainly focusing on thermal effects along the contact zone as temperature is a critical parameter governing the tool–chip interface response and the cutting process.

Attempts have been made to model the contact problem in machining with relatively simple phenomenological laws (Childs, 2006a,b; Arrazola et al., 2008; Filice et al., 2007; Özel, 2006). Most

* Corresponding author at: Laboratoire d'Etude des Microstuctures et de Mécanique des Matériaux, LEM3, CNRS, Université de Lorraine, Ile du Saulcy, 57045 Metz, France. Tel.: +33 3 87 31 53 69; fax: +33 3 87 31 53 66.
E-mail address: molinari@lpmm.univ-metz.fr (A. Molinari).

0020-7683/$ - see front matter © 2012 Elsevier Ltd. All rights reserved.
http://dx.doi.org/10.1016/j.ijsolstr.2012.08.013

Nomenclature

Cutting conditions

V	cutting speed
t_1	uncut chip thickness
α	rake angle
γ	clearance angle
R	cutting edge radius

Chip characteristics

t_2	chip thickness
ϕ	shear angle
τ_Y	shear flow stress of the work material
$\bar{\tau}_{PZ}$	mean shear flow stress along the central line of the primary shear zone
V_c	chip velocity

Tool–chip interface

μ	sliding friction coefficient
$\bar{\mu}$	mean friction coefficient $(=\frac{F_t(rake)}{F_n(rake)})$
μ_{ap}	apparent friction coefficient $(=\frac{F_T}{F_C}$ when $\alpha = 0)$
V_S	sliding velocity
τ	shear stress
σ	normal stress
ξ	exponent controlling the decay of the normal stress along the rake face
σ_0	factor characterizing the level of the normal stress along the rake face
ξ_1	exponent controlling the decay of the shear stress along the rake face
τ_0	factor characterizing the level of the shear stress along the rake face
$\bar{\tau}_{SZ}$	average shear flow stress along the sticking zone
$m_1 = \bar{\tau}_{SZ}/\bar{\tau}_{PZ}$	
l_c	contact length on the flat part of the rake face
l_p	sticking length
l_2	thickness of the secondary shear zone
η	part of frictional heat allocated to the chip along the sliding zone
η_{eff}	effective coefficient of heat partition at the tool–chip interface
κ	thermal conductance of the tool–chip interface
T_1	temperature of the work-material at the entry of the flat part of the rake face
$\hat{T}_1$	temperature of the work-material at the exit of the primary shear zone
$T_{\max}$	maximum temperature of the chip along the rake face
$x_{\max}$	position of the maximum chip temperature on the rake face
$P_e = \frac{V_c l_c}{(k/\rho C_p)}$	Péclet number

Characteristics of the work-material

T_r	reference temperature in the Johnson–Cook law
T_m	melting temperature
$\dot{\varepsilon}_0$	reference strain rate
ρ	mass density
C_p	heat capacity per unit mass
k	heat conductivity
$a = \frac{k}{\rho C_p}$	thermal diffusivity
β	Taylor-Quinney coefficient

Forces

F_C	cutting force
F_T	thrust force
$F_n(rake)$ and $F_t(rake)$	normal and tangential forces exerted by the chip on the flat part of the rake face

Field variables

d^p_{ij}	plastic strain rate tensor
σ_{ij}	Cauchy stress tensor
T	absolute temperature
σ_{eq}	Mises equivalent stress
$\dot{\varepsilon}_{\text{eq}}$	equivalent plastic strain rate
ε_{eq}	cumulated plastic strain

of these laws do not essentially differ from the Coulomb friction law with saturation of the shear stress on the tool face. In the present paper, the tool–chip contact will be modeled by using the pristine Coulomb law. The shear stress on the tool face will appear in our simulations to be naturally saturated by the shear flow stress of the work-material.

The thermo-mechanical characteristics of the work material and of the tool are fixed throughout the whole analysis. The values of the sliding friction coefficient and of the interface thermal resistance are the sole material parameters to be varied. Moreover, a detailed study of the effects of cutting conditions will be performed.

The analysis is for a part based on Finite Element calculations using an Arbitrary Lagrangian Eulerian (ALE) technique. The ALE formulation minimizes element's distortion and is therefore of particular interest in the primary and secondary shear zones and at the vicinity of the cutting edge where large deformations take place. The introduction of ALE technique in the modeling of machining was pioneered by Rakotomalala et al. (1993). This work was followed by different contributions showing the advantages of the ALE formulation in the modeling of machining (Olovsson et al., 1999; Movahhedy et al., 2000, 2002; Adibi-Sedeh and Madhavan, 2003; Özel and Zeren, 2005; Haglund et al., 2005).

The interpretation of numerical results in terms of simple conceptual models and physical laws represents an essential aspect of the present work. Taking advantage of analytical relationships constitutes an efficient route for understanding the complex interactions taking place between model parameters.

Although it does not compose the main goal of the paper, confrontation of the modeling against experimental data is made in several occasions. Ultimately, it is of course wished to establish a machining model from which most of the experimental features could be retrieved. However, in the present state of knowledge of constitutive modeling of metals and of friction phenomena, experimental results are just partially met in most of the works reported in the literature. Therefore, simply reproducing experimental trends and being able to analyze them in a rational way seems to be presently a reasonable intermediate stage before focusing on close quantitative agreement.

This work is devoted to the analysis of contact variables (stress and temperature fields at the tool–chip interface, particle velocities, sticking length, thickness of the secondary shear zone, hot spot position). The response of the work material in the vicinity of the tool–chip interface appears to be a crucial factor controlling the contact problem. The effects of cutting conditions and of frictional properties on contact stresses and contact temperatures are analyzed. A law governing the heating of the chip on the rake face is proposed and evaluated against numerical simulations. Characterizing the heating of the chip is essential as it was demonstrated by Molinari et al. (2011) that, whatever the cutting

conditions considered, the overall friction coefficient (accounting for both sliding and sticking contact) is solely function of the maximum chip temperature at the rake face.

The present analysis of local contact variables offers the possibility of improving the analytical modeling of cutting processes. It provides also the knowledge on how local contact variables are influenced by cutting conditions and friction characteristics. Characterizing local variables is useful for analyzing the tool wear and the tool-edge failure due to the combined effects of high pressure and the reduction of the material strength by heating.

The paper is organized as follows. The basic equations of the problem and the numerical model are presented in Section 2. The material properties of the work-material are taken as representative of a medium carbon steel 42CrMo4 (AFNOR: 42CD4). The properties of the work-material are fixed in the entire paper. A parametric analysis is performed where we vary the values of the sliding friction coefficient, of the cutting speed, of the feed, of the tool edge radius and of the thermal resistance of the tool–chip interface. Data concerning the stress and temperature distributions along the tool–chip interface, the contact length and the sticking length, are analyzed in the rest of the paper.

Distributions of stresses and of particle velocity along the tool–chip interface are studied in Section 3 and the consistency with respect to the contact law is checked. Heating and thermal softening along the tool–chip interface are analyzed in Section 4 and are correlated to the evolution of the shear flow stress along the sticking zone. The contributions to interfacial heating of parameters such as contact length, shear stress and chip velocity are characterized numerically and correlated to analytical formulation. Similarly, we identify the position of the hot spot on the tool–chip interface. The role of the thermal resistance of the interface is discussed. Experimental trends for temperature recently obtained by Sutter and Ranc (2007) at high cutting velocities on a ballistic machining set-up, are compared to our theoretical predictions. The morphology of the secondary shear zone (SSZ) is characterized in Section 5. The effects of the cutting speed are summarized in Section 6, with a special emphasis on the asymptotic regime (for which the process variables are found to be weakly dependent of cutting speed and feed) that occurs at relatively high cutting velocities (larger than 10 m/s) for values of the sliding friction coefficient larger than 0.4. This asymptotic state is shown to be the manifestation of a boundary layer regime due to the increase (at high cutting speeds) of the chip temperature towards the melting temperature of the work-material.

2. Basic equations and numerical modeling

The framework adopted for the modeling of orthogonal cutting is presented in this section.

2.1. Constitutive equation of the work material and heat generation

The work material is a medium carbon steel 42CrMo4 (AFNOR: 42CD4) with chemical composition given in Sutter and Molinari (2005). The material behavior is modeled by using the Johnson–Cook law:

$$\sigma_{eq} = \left[A + B\varepsilon_{eq}^{n}\right]\left[1 + C\ln\left(\frac{\dot{\varepsilon}_{eq}}{\dot{\varepsilon}_0}\right)\right]\left[1 - \left(\frac{T - T_r}{T_m - T_r}\right)^{m}\right] \quad (1)$$

σ_{eq} and $\dot{\varepsilon}_{eq}$ are respectively the Mises equivalent stress and strain rate, T is the absolute temperature, T_r a reference temperature (the room temperature here), T_m the melting temperature, $\dot{\varepsilon}_0$ a reference strain rate. The plastic flow is assumed to be governed by the J_2-flow theory.

The parameters of the Johnson–Cook law were identified experimentally by Molinari et al. (1997) and are reported in Table 1. Thermo-mechanical properties were characterized with a universal hydraulic machine for quasi-static tests and with Hopkinson bars for the dynamic response. Other mechanical and thermal properties of the work material and of the tool material are given in Table 2. An uncoated carbide tool is considered. It is assumed to behave elastically.

The evolution of the temperature of the work-material is governed by the energy equation:

$$\rho C_p \dot{T} - k\Delta T = \beta d_{ij}^{p}\sigma_{ij} \quad (2)$$

$\dot{T}$ is the material derivative of the temperature, ΔT is the Laplacian of T, d_{ij}^{p} are the components of the plastic strain rate tensor and σ_{ij} the components of the Cauchy stress tensor. ρ, C_p and k are respectively the mass density, the heat capacity per unit mass and the heat conductivity of the work material. The thermal properties C_p and k are considered as constants in this analysis (temperature dependence neglected).

The Taylor-Quinney coefficient, β, is in general rate and strain dependent and is function of the metal considered. In their experiments on iron, Rittel et al. (2006) reported that the maximum value of β (close to unity) is observed at strain rates larger than $10^4\ s^{-1}$. Usually, β increases also with strain and approaches unity at very large strains. As large strain rates and strains are encountered in machining within the primary and secondary shear zones, it is justified to assign to β a large value close to unity. In our modeling, the fixed value $\beta = 0.9$ is considered, but the trends in the results would remain essentially unchanged by varying the Taylor-Quinney coefficient in a range of values close to unity.

At the tool–chip interface, the frictional energy per unit time and unit surface is equal to τV_S along the sliding zone, with τ being the shear stress and V_S the sliding velocity. Frictional energy vanishes when sticking occurs ($V_S = 0$). It is assumed that the totality of the frictional energy is transformed into heat. The proportion of the frictional heat energy allocated to the chip is characterized by the coefficient of heat partition η ($0 \leqslant \eta \leqslant 1$). A detailed analysis of the contact mechanics at the scale of surface asperities would be needed to characterize the value of η along the sliding zone. Such study could be based on Finite Element simulations at the microscale (level of asperities) coupled with molecular dynamics simulations. In the absence of precise information, the value $\eta = 0.5$ is adopted in the present calculations. Thus, along the sliding zone, frictional heat is equally allocated to the two bodies in contact. However, it should be noted that, just after being deposited in chip and tool, the frictional heat is redistributed through the tool–chip interface if the thermal conductance of the interface is non-zero.

The thermal conductance of the tool–chip interface has the value $\kappa = 2000\ W\,m^{-2}\,K^{-1}$ in most of our calculations. Under the high contact pressures generated in the cutting process, κ may have larger values (low thermal resistance of the interface). Therefore, the effect of a large thermal conductance κ will be explored by considering the value $\kappa = 10^9\ W\,m^{-2}\,K^{-1}$. Let us note that the temperature is discontinuous across the tool–chip interface except if $\kappa = \infty$ (no thermal resistance).

The free surface of the workpiece and of the chip and the external boundary of the tool are assumed to be adiabatically insulated.

Table 1
Material parameters of the Johnson–Cook model for the 42CrMo4 steel, according to Molinari et al. (1997).

A (MPa)	B (MPa)	C	n	$\dot{\varepsilon}_0$ (s^{-1})	m	T_r (K)	T_m (K)
612	436	0.008	0.15	5.77 E^{-4}	1.46	293	1793

Table 2
Mechanical and thermal parameters of the work-material (42CrMo4 steel) and of the carbide tool. E, Young modulus, ν, Poisson ratio, ρ, mass density, C_p, heat capacity per unit mass, k, heat conductivity, β, Taylor-Quinney coefficient.

	E (GPa)	ν	ρ (kg m^{-3})	C_p (m^2 s^{-2} K^{-1})	k (N K^{-1} s^{-1})	β
Work material	202	0.3	7800	500	54	0.9
Tool	1000	0.3	12700	234	33.5	–

The dimension of the tool is taken large enough, so that the heating at the tool–chip interface is not affected by the thermal conditions at the external boundary of the tool.

2.2. Friction law

The Coulomb law is used to model contact. Under sliding condition, the shear stress τ is related to the normal stress σ by the relationship:

$$\tau = \mu\sigma \tag{3}$$

where μ is the sliding friction coefficient (taken as constant along the interface). The sliding velocity vanishes when $\tau < \mu\sigma$. In machining, the latter condition is realized at the vicinity of the tool tip, where the normal stress reaches high values. Then, sticking occurs between chip and tool.

Along the sticking zone, the work material is plastically sheared and the shear stress at the tool–chip interface is identical to the shear flow stress of the work-material τ_Y which is function of temperature, strain and strain rate. Thus the contact is basically governed by two parameters. The first parameter (the sliding friction coefficient μ) relates to an intrinsic interface characteristic, the second refers to a mechanical property of the work-material (τ_Y). It turns out that:

$$\tau = \inf(\tau_Y, \mu\sigma) \tag{4}$$

Zorev (1963) considered the relationship (4) as being the constitutive law of the interface. This model was implemented in Finite Element simulations of orthogonal cutting, see for example Marusich and Ortiz (1995). Arrazola and Özel (2010) have recently explored the effect of a limit shear stress τ_{limit} in the contact law (τ_Y being replaced by τ_{limit} in Eq. (4)).

The genuine Coulomb law is used in the present work. The shear stress along the sticking zone will be found to be equal to τ_Y as an outcome of the calculations.

A more general friction law than (4) was introduced in the literature related to machining, Childs (2006b), Filice et al. (2007), Childs et al. (1998), Dirikolu et al. (2001):

$$\tau = \tau_Y\left(1 - \exp\left(-\left(\frac{\mu\sigma}{\tau_Y}\right)^n\right)\right)^{\frac{1}{n}} \tag{5}$$

where n is an arbitrary positive parameter. This law was initially proposed by Shiratashi and Usui (1976) for $n = 1$. It should be noted that for small values of σ Eq. (5) reduces to the form (3) of the Coulomb law for sliding contact while for large values of σ the relationship $\tau = \tau_Y$ corresponding to sticking contact is retrieved. Thus, the law (5) offers a smooth transition from sliding to sticking contact when σ varies. However this transition is based on the phenomenological relationship (5) which has no specific physical meaning.

2.3. Numerical modeling

The problem of orthogonal cutting is modeled by Finite Element simulations using the code ABAQUS/Explicit (2003) and the ALE formulation with the boundary specifications shown in Fig. 1. Geometrical characteristics of the cutting model are reported in Fig. 2.

For some materials chip segmentation is experimentally observed at high cutting speeds. This feature cannot be accounted for with the ALE formulation. Only stationary flow and continuous chip formation can be simulated in this framework. Thus, some of the results obtained with the present numerical model may not be in total agreement with experimental observations made at very high cutting speeds. However, when chip segmentation is due to adiabatic heating, we believe that the main trends are conserved if the band spacing is wide enough. In that case, the appearance of shear bands within the chip is characterized by discrete events which should not affect significantly the average values of field variables.

Plane-strain deformations are assumed in the modeling. An example of mesh configuration is shown in Fig. 1. CPE4RT quadrilateral elements with reduced integration were used. They have four nodes, are adapted for plane deformation applications and they account for temperature effects.

In most of calculations the mesh size was about 4 μm. A mesh sensitivity analysis was performed by reducing the average mesh size to 2 μm. Little differences were found in the results as will be shown later. Therefore, to optimize computational time, the mesh size of 4 μm was generally adopted, except for some cases where a finer mesh of 2 μm was used (e.g. for the evaluation of the thickness of the secondary shear zone).

In the Abaqus software, two options are offered to model the contact problem: the kinematic and the penalty algorithms. Numerical tests conducted with the Coulomb friction law showed significant variations in the results according to the choice of the contact algorithm Results obtained with the kinematic formulation presented some inconsistencies. For example, when sliding occurred, the ratio τ/σ was found to be different from the friction coefficient μ. Therefore, calculations were made by using the penalty (and surface/surface) method which provides consistent results.

2.4. Parametric analysis

The sliding friction coefficient μ is assumed to be constant, i.e. independent from cutting conditions and from field variables.

All results correspond to quasi-steady regimes reached when the interface temperature and the values of cutting forces are nearly time independent. Time histories of cutting and thrust forces and other cutting variables reveal that a quasi-steady state regime is obtained after a short transient period. For instance, for the test corresponding to the following conditions: $\mu = 0.8$, $V = 8$ m/s, $t_1 = 0.1$ mm, $R = 0.015$ mm, $\kappa = 2000$ W m^{-2} K^{-1}, the quasi-steady regime is reached for a time of about 500 μs.

The numerical approach and the cutting problem is the same as in Molinari et al. (2011). The pertinence of the numerical model was checked in Molinari et al. (2011) against various experimental results obtained for the medium carbon steel 42CrMo4. In particular, the measured values of overall friction coefficients and their variation with cutting conditions were correlated to numerical data.

A parametric analysis is conducted by varying the value of the sliding friction coefficient in the range $0 \leqslant \mu \leqslant 1$ and by changing cutting conditions. The values of the rake and clearance angles are

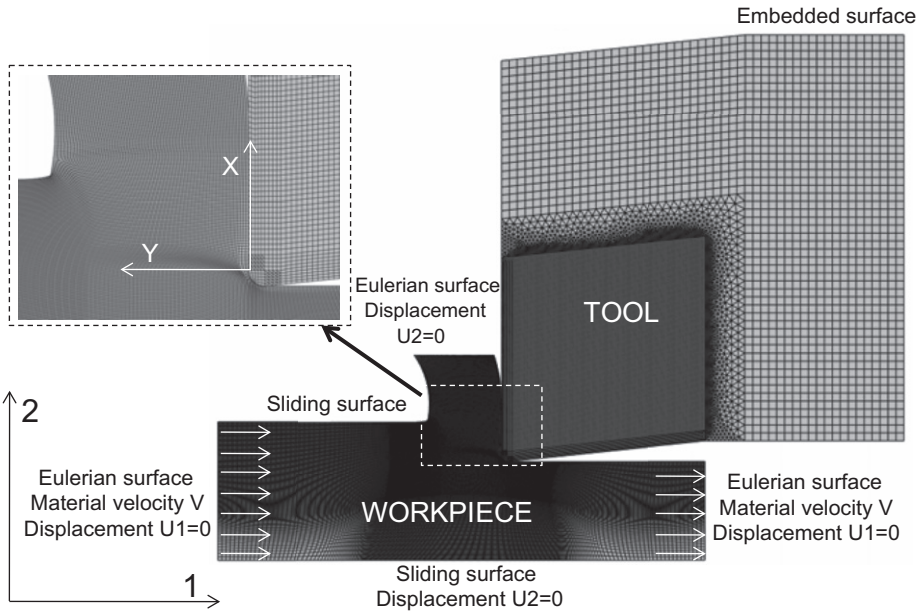

Fig. 1. Deformed mesh and conditions imposed in the ALE model.

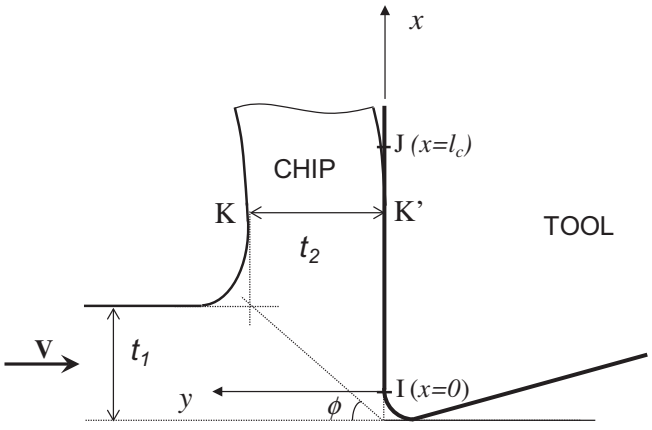

Fig. 2. Geometrical characteristics of the cutting model.

fixed ($\alpha = 0, \gamma = 7^\circ$). Cutting conditions are summarized in Table 3. The labels T4, T5 and T6 in the first column of Table 3 refer to similar calculations reported respectively in Tables 4-5-6 of Molinari et al. (2011). In the present paper, the focus is made on the analysis of local variables and on the solution of the thermal problem at the tool chip interface.

Values of T_1 and of T_{max} corresponding respectively to the nodal temperature of the work-material at I ($x = 0$), see Fig. 2, and to the maximum nodal temperature of the work-material along the tool–chip interface are of special interest for the analysis of the thermal problem.

The results corresponding to test conditions K of Table 3 are reported in Table 4. Two different values of the thermal conductance of the tool–chip interface are considered: $\kappa = 2000$ W m^{-2} K^{-1} and $\kappa = 10^9$ W m^{-2} K^{-1}. It is worth noting that a fine mesh size (about 2 μm) was used while the mesh size was about 4 μm for other calculations (T4, T5, T6) of Table 3. Thus, in addition to the effects of κ, results of Table 4 will allow us to evaluate the mesh sensitivity by direct comparison with data related to T4 for $\kappa = 2000$ W m^{-2} K^{-1}. More details about mesh sensitivity are given in Section 4.5.

3. Stress and velocity distributions along the tool rake face

We first characterize sliding and sticking contact by investigating the distribution along the tool rake-face of the sliding velocity V_S, as shown in Fig. 3a for the test T4 of Table 3 with friction coefficient $\mu = 0.8$ and cutting speed $V = 8$ ms^{-1}. The tool is fixed and V_S is the component of the particle velocity tangential to the rake-face. The origin of the x-axis is located at the point I, see Fig. 2. The results of Fig. 3a reveal the existence of (i) a sticking zone where the sliding velocity V_S is nearly zero, (ii) a sliding zone where $V_S \neq 0$. Note the progressive increase of the sliding velocity from nearly zero at the exit of the sticking zone, to the quasi-steady value 4 m/s. Fig. 3b shows the distribution along the tool–chip interface of the normal stress σ (actually $\mu\sigma$ is represented) and of the shear stress τ (nodal values for σ and τ). By convention σ is taken as positive; thus, σ is the absolute value of the real normal stress. σ vanishes at $x = l_c$, where $l_c = 0.267$ mm is the length of the contact zone. The sliding zone is defined by $l_p < x < l_c$. The length of the sticking zone is given in Fig. 3a by $l_p = 0.174$ mm. The results of

Table 3
Values of the cutting parameters and of interface properties used in simulations; α rake angle, γ clearance angle, η heat partition coefficient, μ sliding friction coefficient, t_1 uncut chip thickness, R cutting edge radius, V cutting speed, κ thermal conductance of the tool–chip interface.

Test label	μ	t_1 (mm)	V (ms^{-1})	R (mm)	κ (W m^{-2} K^{-1})
$\alpha = 0^\circ, \gamma = 7^\circ, \eta = 0.5$					
T4	$0 \leqslant \mu \leqslant 1$	0.1	$1 \leqslant V \leqslant 50$	0.015	2000
T5	0.8	0.1	$4 \leqslant V \leqslant 30$	0.030	2000
T6	0.6	$0.05 \leqslant t_1 \leqslant 0.5$	$4 \leqslant V \leqslant 40$	0.015	2000
K	0.6	0.1	$6 \leqslant V \leqslant 50$	0.015	2000 and 10^9

Table 4
Results corresponding to test conditions K of Table 3 are reported here for various values of the cutting speed V. Definitions of other variables are found in the nomenclature. Calculations are conducted with a mesh size of about 2 μm while for tests T4, T5 and T6 of Table 3 the mesh size was 4 μm. Two values of the thermal conductance κ of the tool chip interface are considered.

Test label	κ (W/m^2/K)	V (m/s)	F_C (kN/m)	F_T (kN/m)	μ_{ap}	F_n (*rake*) (kN/m)	F_t (*rake*) (kN/m)	$\bar{\mu}$	$\bar{\tau}_{PZ}$ (MPa)	$\bar{\tau}_{SZ}$ (MPa)	t_2 (mm)	l_c (mm)	l_p/l_c	ϕ (deg)	$T_{\max}$ (K)	T_1 (K)	$x_{\max}/l_c$
$t_1 = 0.1$ mm, $R = 0.015$ mm, $\mu = 0.6$																	
K01	2000	6	254	131	0.515	221	104	0.471	629	440	0.275	0.265	0.696	20.0	1363	997	0.708
K02	2000	10	226	105	0.464	192	74.7	0.390	641	406	0.229	0.213	0.727	23.6	1452	1026	0.734
K03	2000	15	214	90.8	0.424	181	61.3	0.339	645	354	0.211	0.193	0.741	25.4	1526	1073	0.762
K04	2000	20	207	83.4	0.404	174	53.5	0.308	651	327	0.197	0.182	0.742	26.9	1565	1100	0.751
K05	2000	30	197	72.3	0.367	163	41.2	0.252	656	270	0.184	0.167	0.760	28.5	1626	1174	0.736
K06	2000	50	192	65.0	0.339	157	32.6	0.207	661	238	0.168	0.154	0.760	30.8	1682	1244	0.775
K07	10^9	6	261	146	0.559	231	121	0.524	624	478	0.283	0.269	0.654	19.3	1281	998	0.833
K08	10^9	10	231	115	0.498	204	91.0	0.446	639	437	0.244	0.233	0.709	22.3	1401	1028	0.854
K09	10^9	15	219	99.4	0.454	178	63.2	0.355	648	427	0.178	0.168	0.720	29.3	1472	1025	0.834
K10	10^9	20	230	92.2	0.402	183	51.5	0.282	656	370	0.173	0.162	0.748	30.0	1540	1065	0.847
K11	10^9	30	204	80.8	0.396	169	49.5	0.292	659	315	0.189	0.175	0.754	27.9	1610	1145	0.886
K12	10^9	50	198	71.5	0.361	165	40.3	0.245	662	273	0.185	0.170	0.751	28.4	1683	1210	0.880

Fig. 3b show that $\tau = \mu\sigma$ in the sliding zone, in agreement with the Coulomb friction law.

It is worth analyzing the nature of the plastic flow along the sticking zone. Firstly, it should be noted that the particle velocity being zero at the tool–chip interface, the global chip movement must be accommodated by a shear layer (secondary shear zone) where the chip undergoes plastic flow. Apart from numerical oscillations, the results of Fig. 3c reveal that, along the sticking zone, the shear stress τ is related to the Mises-equivalent stress σ_{eq} (evaluated at Gauss integration point) through the relationship:

$$\tau = \frac{\sigma_{eq}}{\sqrt{3}} \tag{6}$$

It is shown in Appendix A that, for a material obeying the Mises-J_2 flow theory, the condition (6) is satisfied if and only if the plastic flow along the tool–chip interface is simple shearing. It should be also noted that plastic flow occurs when $\sigma_{eq} = \sqrt{3}\tau_Y$, with τ_Y being the shear flow stress. Therefore, it is found by considering (6) that the shear stress is identical to the shear flow stress along the sticking zone:

$$\tau = \tau_Y \tag{7}$$

The present numerical modeling of contact appears to be in agreement with the contact model proposed by Zorev (1963) assuming that the condition (7) is satisfied along the sticking zone.

It is observed in Fig. 3c that the relationship (7) is not met along the sliding zone. Flow analysis within the chip indicates that plastic deformation is weakly activated along the sliding zone. However, according to the results demonstrated in Appendix A, the mode of plastic deformation is not simple shearing since $\tau \neq \frac{\sigma_{eq}}{\sqrt{3}}$. The plastic activity along the sliding zone may be related to chip curling.

The contact regime depends on the value of the sliding friction coefficient μ. While results of Fig. 3 were related to $\mu = 0.8$, a small sliding friction coefficient, $\mu = 0.2$, is considered in Fig. 4. Cutting conditions are the same as for Fig. 3. It appears from Fig. 4a that sticking does not exist anymore for $\mu = 0.2$. The chip slides along the tool rake-face with a velocity of about 4—5 ms^{-1}. Stress profiles displayed in Fig. 4b indicate an excellent consistency of the numerical results with the Coulomb friction law $\tau = \mu\sigma$. The distribution of $\sigma_{eq}/\sqrt{3}$ is shown in Fig. 4c. The fact that $\sigma_{eq}/\sqrt{3} > \tau$ is an indication that the mode of deformation along the rake face is not plastic shearing. Additional information is provided by the examination of numerical results. It is observed that the cumulated plastic deformation increases with x along the rake face. Thus, the chip is plastically deformed along the rake face (chip curling) and from the J_2-flow theory it follows that $\sigma_{eq}/\sqrt{3}$ is identical to the shear flow stress τ_Y. Finally, it turns out from these theoretical considerations that $\tau_Y > \tau$ all along the tool–chip interface (sliding contact). The same conclusion was obtained for the results of Fig. 3c ($\mu = 0.8$) along the sliding zone.

From this discussion, the results appear to be fully consistent with the Coulomb contact law along the sliding zone and to provide the correct physics along the sticking zone. It is so for the whole series of calculations reported in this paper. Further consistency is found by checking in Appendix B that the chip velocity obtained numerically is in agreement with plastic flow incompressibility.

Experimental measurements of stress distributions along the tool face are difficult to achieve. Therefore, comparing experiments with theoretical predictions is not easy. However, it can be mentioned that experimental stress profiles reported by Childs et al. (1989) are in qualitative agreement with the simulated stress distributions given in Fig. 3b.

The variations of σ and τ along the tool–chip interface are displayed in Fig. 5 for various values of the cutting speed and of the sliding friction coefficient corresponding to tests T4 of Table 3. For completeness, the stress distributions are displayed by including the tool edge region using the following representation. Consider on the tool edge a given point P of coordinates (x, y) (see axes in Fig. 2) and denote by σ the absolute value of the normal stress at P and by τ the shear stress at the interface. To P we associate the point (x, σ) (or (x, τ)) in the Fig. 5a. Note that we have $-R \leqslant x \leqslant 0$, for the points located on the tool edge, with $R = 0.015$ mm being the edge radius. The edge region provides always a larger stress level.

4. Heating and thermal softening along the tool–chip interface

4.1. Temperature distribution along the tool–chip interface

The value $\kappa = 2000$ W m^{-2} K^{-1} is assigned to the thermal conductance of the tool–chip interface. The effect of a larger value of κ will be evaluated in Section 4.5. For the low value of κ considered here, the temperature is discontinuous at the interface. Therefore the temperature on the chip side T^{int}_{chip} should be distinguished from those on the tool side T^{int}_{tool}. However, the relevant parameter for the modeling of the cutting process is T^{int}_{chip}. As a matter of fact, the chip temperature at the interface controls the thermal softening of the work-material and thereby does affect the whole process. This is the reason why the present analysis is focusing on T^{int}_{chip}. For conciseness, this temperature will be denoted as interface temperature, T^{int}.

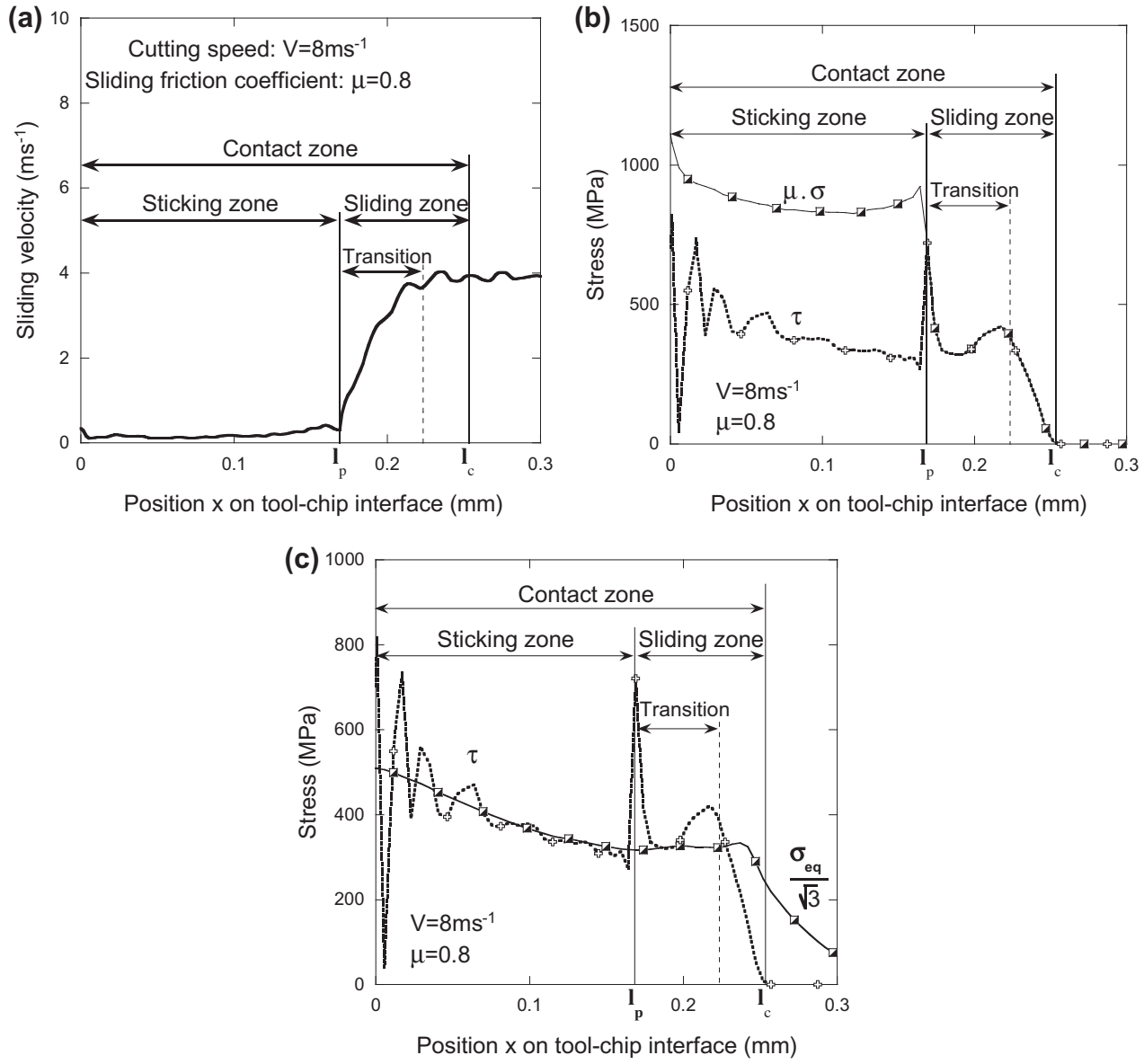

Fig. 3. Field variables at the tool rake face for $\mu = 0.8$ and $V = 8$ ms^{-1} (other conditions are relative to tests T4 of Table 3): (a) distribution of the sliding velocity V_S along the tool–chip interface. For the large value of μ considered here, we note the existence of a sticking zone ($V_S \approx 0$) with length $l_p = 0.174$ mm. The origin of the x-axis is located at the extremity I of the flat part of the tool rake face, see Fig. 2. (b) Distribution of the shear stress τ and of $\mu\sigma$ along the tool–chip interface. The end of contact corresponds to the vanishing of the stress at $x = l_c = 0.267$ mm. The results are in agreement with the Coulomb law ($\tau = \mu\sigma$ along the sliding zone and $\tau < \mu\sigma$ along the sticking zone). (c) Distribution along the tool–chip interface of the shear stress τ and of $\sigma_{eq}/\sqrt{3}$. The fact that these quantities are well correlated for $0 \leqslant x \leqslant l_p$ is an indication that the mode of plastic deformation along the tool face is simple shearing when sticking occurs.

The temperature distribution along the tool rake face is shown in Fig. 6 for the cases considered in Fig. 3 (high friction, $\mu = 0.8$) and Fig. 4 (low friction, $\mu = 0.2$). As expected, the interface temperature is smaller for the lower value of friction. The increasing of temperature at the tool face results from (i) self-heating of the work material due to plastic deformation within the primary and secondary shear zones, (ii) frictional heating along the sliding zone. The temperature T_1 at the point I (see Fig. 2) is the result of the heating associated to plastic deformation near the tool tip. This temperature appears to be larger for $\mu = 0.8$ (T_1 = 1010 K) than for $\mu = 0.2$ (T_1 = 854 K). It is worth noticing that T_1 is significantly different from the temperature $\hat{T}_1$ evaluated at the exit of the primary shear zone on the path P_1P_2 shown in Fig. 20 of Appendix C: $\hat{T}_1 = 645$ K for $\mu = 0.8$ and $\hat{T}_1 = 613$ K for $\mu = 0.2$. The increasing of the temperature for a material particle crossing the primary shear zone is basically related to adiabatic plastic shearing as discussed in Appendix C. The plastic deformation field which produces the increasing of the temperature at I is more complex than along the path P_1P_2 (partly because of the tool radius effect) and cannot be easily represented by analytical means.

Beyond x = 0 (point I), a further increasing of temperature is observed along the tool face. For $\mu = 0.8$ (test T4 of Table 3, with $V = 8$ ms^{-1}) the temperature evolves from T_1 = 1010 K to the maximum value T_{max} = 1402 K, Fig. 6a. This increasing is due to the dissipation of plastic work along the sticking zone. The maximum temperature T_{max} is reached at the end of the sticking zone at $x_{max} = l_p = 0.174$ mm. There is no increasing of temperature in the sliding zone, rather a drop of 150° is observed between x_{max} and the end of contact. This drop is the consequence of heat transfer towards the surrounding (chip and tool) which cannot

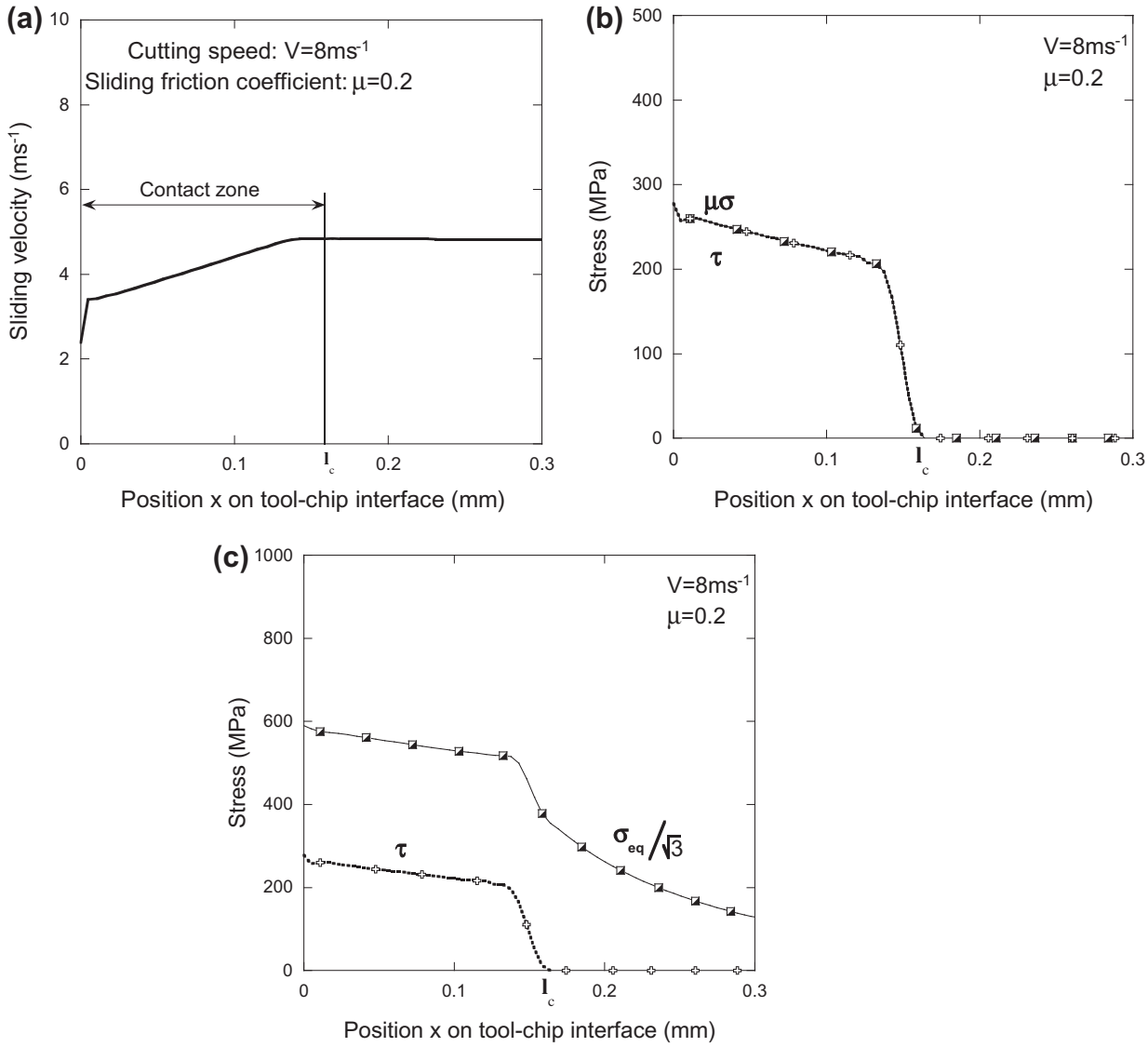

Fig. 4. Field variables at the tool rake face for $\mu = 0.2$ and $V = 8$ ms^{-1} (other conditions are relative to tests T4 of Table 3). In contrast to Fig. 3, a small value of the sliding friction coefficient is adopted here. The following results are displayed: (a) distribution of the sliding velocity V_S, showing that sliding occurs all along the tool–chip interface, (b) Identical distributions of the shear stress τ and of $\mu\sigma$ indicating that the friction Coulomb law (in sliding regime) is perfectly satisfied along the tool–chip interface. The contact length is $l_c = 0.164$ mm. (c) Distinct distributions of the shear stress τ and of $\sigma_{eq}/\sqrt{3}$ revealing that there is no plastic shearing along the tool–chip interface.

be compensated by the low level of frictional heating along the sliding zone (as the level of shear stress is rapidly decreasing at large values of x).

For $\mu = 0.2$, there is no sticking and $T_{max} = 980$ K occurs at $x_{max} = 0.127$ mm near the end of the contact zone ($l_c = 0.164$ mm) see Fig. 6b. There is no secondary shear zone, and the increasing of the temperature up to T_{max} appears as the sole result of frictional heating.

The influence of the cutting speed on the temperature distribution is illustrated in Fig. 6c for $\mu = 0.8$ and in Fig. 6d for $\mu = 0.2$. Of note is the increasing of T_{max} with V. The position x_{max} of T_{max} appears to be nearly insensitive to the cutting speed for the low value of friction $\mu = 0.2$, while for $\mu = 0.8$, x_{max} is moving significantly towards the tool tip when V is increased. This is in keeping with the decreasing of the contact length when the cutting speed is augmented. These results will be further commented in the following sections. In particular, the position x_{max} will be correlated with the stress distribution on the tool–chip interface.

The dependence of T_{max} upon cutting speed is illustrated in Fig. 6e for various values of μ. Two regimes can be distinguished. For low values of the sliding friction coefficient ($\mu = 0$, $\mu = 0.2$) sliding contact occurs all along the tool rake face ($x \geqslant 0$). In that case T_{max} appears to be an increasing function of μ, as the amount of frictional heating is more important at higher friction. However, for large values of μ, contact is dominated by sticking and the "interface" response is mainly controlled by the flow stress of the work-material with a minor effect of μ.

The transition between sliding contact and sticking dominated contact is clearly apparent for $\mu = 0.4$. For cutting speeds smaller than 8 ms^{-1} we have pure sliding ($l_p = 0$, tests #31–35 of Table 4 of Molinari et al. (2011)). For larger cutting speeds, the contact is dominated by sticking and values of T_{max} merge with those obtained for $\mu \geqslant 0.6$. The appearance of a saturation regime for large values of μ and large cutting velocities is an important feature which will be further discussed.

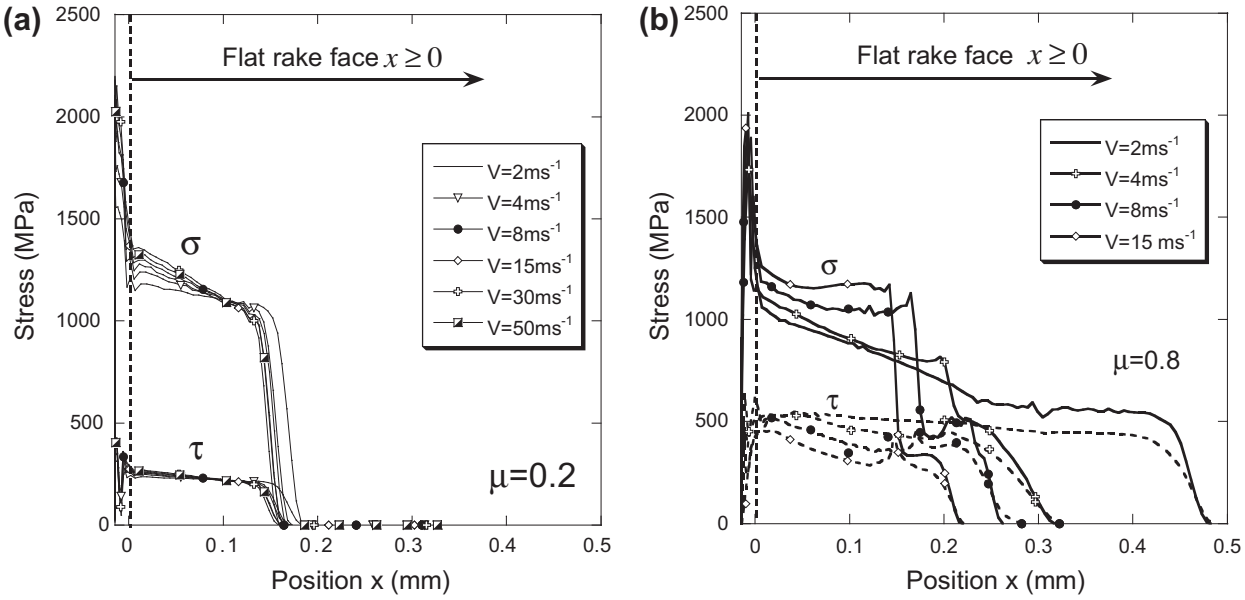

Fig. 5. Distributions of the normal and shear stresses on the tool–chip interface, including the round edge of the tool, for various values of the cutting speed and of the sliding friction coefficient. Conditions are related to tests T4 of Table 3. Evolution of stress profiles with the cutting speed for (a) $\mu = 0.2$ and (b) $\mu = 0.8$.

The same observations can be made for the temperature T_1, see Fig. 6f. It is worth noting that T_1 becomes weakly dependent upon V when the contact is dominated by sticking i.e. when $\mu > 0.4$. This is also the case for $\mu = 0.4$ and $V \geqslant 8$ ms^{-1}.

4.2. Thermal softening at the tool–chip interface

The effect of thermal softening due to heating of the chip along the tool face can be quantitatively evaluated by using the multiplicative form of the Johnson–Cook law: $\sigma_{eq} = f(\varepsilon_{eq})g(\dot{\varepsilon}_{eq})h(T)$. Considering for example the case $\mu = 0.8$, the drop of the shear flow stress by 200 MPa along the sticking zone observed in Fig. 3c appears to be mostly controlled by the increasing of temperature $T_{max} - T_1 = 392$ K, see Appendix D.

When increasing the cutting speed, the heating at the tool–chip interface is enhanced and the shear flow stress along the sticking zone is reduced by the effect of thermal softening. This feature is illustrated in Fig. 7a representing the evolution of the mean shear flow stress, $\bar{\tau}_{SZ}$, along the sticking region (secondary shear zone) in terms of the cutting speed V for various values of μ. $\bar{\tau}_{SZ}$ is defined by

$$\bar{\tau}_{SZ} = \frac{1}{l_p}\int_0^{l_p} \tau(x)dx \tag{8}$$

and is calculated by taking the nodal values of τ on a path following the tool–chip interface.

Fig. 7a shows also the variation of $\bar{\tau}_{PZ}$ (mean shear flow stress in the primary shear zone) and the evolution of the ratio $m_1 = \bar{\tau}_{SZ}/\bar{\tau}_{PZ}$. $\bar{\tau}_{PZ}$ is evaluated along the central line of the primary shear zone (see Molinari et al. (2011)). The stress $\bar{\tau}_{PZ}$ exhibits weak variations with cutting speed and friction μ. This observation is general and can be checked from the results reported in Molinari et al. (2011). Therefore, the variation of m_1 is mostly due to $\bar{\tau}_{SZ}$. In the literature, the value $m_1 = 0.8$ is frequently considered to be representative of thermal softening along the secondary shear zone. It is seen here that m_1 varies significantly in terms of the cutting speed from about 0.9 at $V = 2$ ms^{-1} to 0.5 at $V = 50$ ms^{-1}.

As shown in Appendix D, the evolution of the shear flow stress along the sticking contact is mostly controlled by the increasing of temperature. This suggests that $\bar{\tau}_{SZ}$ could be related to a characteristic interface temperature by a one-to-one correspondence. In Fig. 7b we have reported $\bar{\tau}_{SZ}$ in terms of T_{max} for all the tests T4 of Table 3 ($t_1 = 0.1$ mm) for which sticking is activated ($l_p \neq 0$). Tests T6 performed for other values of the uncut chip thickness ($t_1 = 0.05$ mm, $t_1 = 0.25$ mm and $t_1 = 0.5$ mm) are also reported. It is interesting to observe that for such a variety of cutting speeds (1 ms$^{-1} \leqslant V \leqslant 50$ ms^{-1}), feeds and values of the sliding friction coefficient ($0.4 \leqslant \mu \leqslant 1$), all points are more or less forming a single "master curve". This curve can be seen as defining the "constitutive response" of $\bar{\tau}_{SZ}$ in terms of the single parameter T_{max}. Such constitutive relationship is an important feature for the development of machining models. It is worth noting that by extrapolating the data reported in Fig. 7b the master curve would intersect the abscissa-axis at a point slightly above the melting temperature of the work material $T_m = 1793$ K. This corresponds to the loss of the resistance to shear of the tool–chip interface caused by the melting of the work-material.

4.3. Analytical characterization of the heating at the tool–chip interface

T_{max} appears as an important parameter controlling the cutting process through the evolution of the mean shear flow stress $\bar{\tau}_{SZ}$ along the sticking zone. Furthermore, it has been demonstrated by Molinari et al. (2011) that the dependence of the apparent friction coefficient μ_{ap} with respect to cutting conditions can be also expressed in terms of the sole parameter T_{max}. The apparent friction coefficient is defined as $\mu_{ap} = \frac{F_T}{F_C}$ (since $\alpha = 0$) with F_C and F_T being respectively the cutting and thrust forces. In view of the importance of T_{max} in the modeling of the cutting process, it is worth trying to evaluate this temperature by analytical means.

When the cutting speed V is increased, the chip temperature at the tool–chip interface sustains in general an important growth. This point was illustrated for T_{max} in Fig. 6e. Evolutions with V of the temperature T_1 at I and of $T_{max} - T_1$ are reported in Fig. 8 for $\mu = 0.8$ and $\mu = 0.2$. Tests conditions correspond to T4 in Table 3. $T_{max} - T_1$ is the increase of the chip temperature between the beginning of the rake face I ($x = 0$) and the point x_{max} of maximum temperature. This temperature increase is a manifestation of either dissipation associated to plastic shearing along the interface

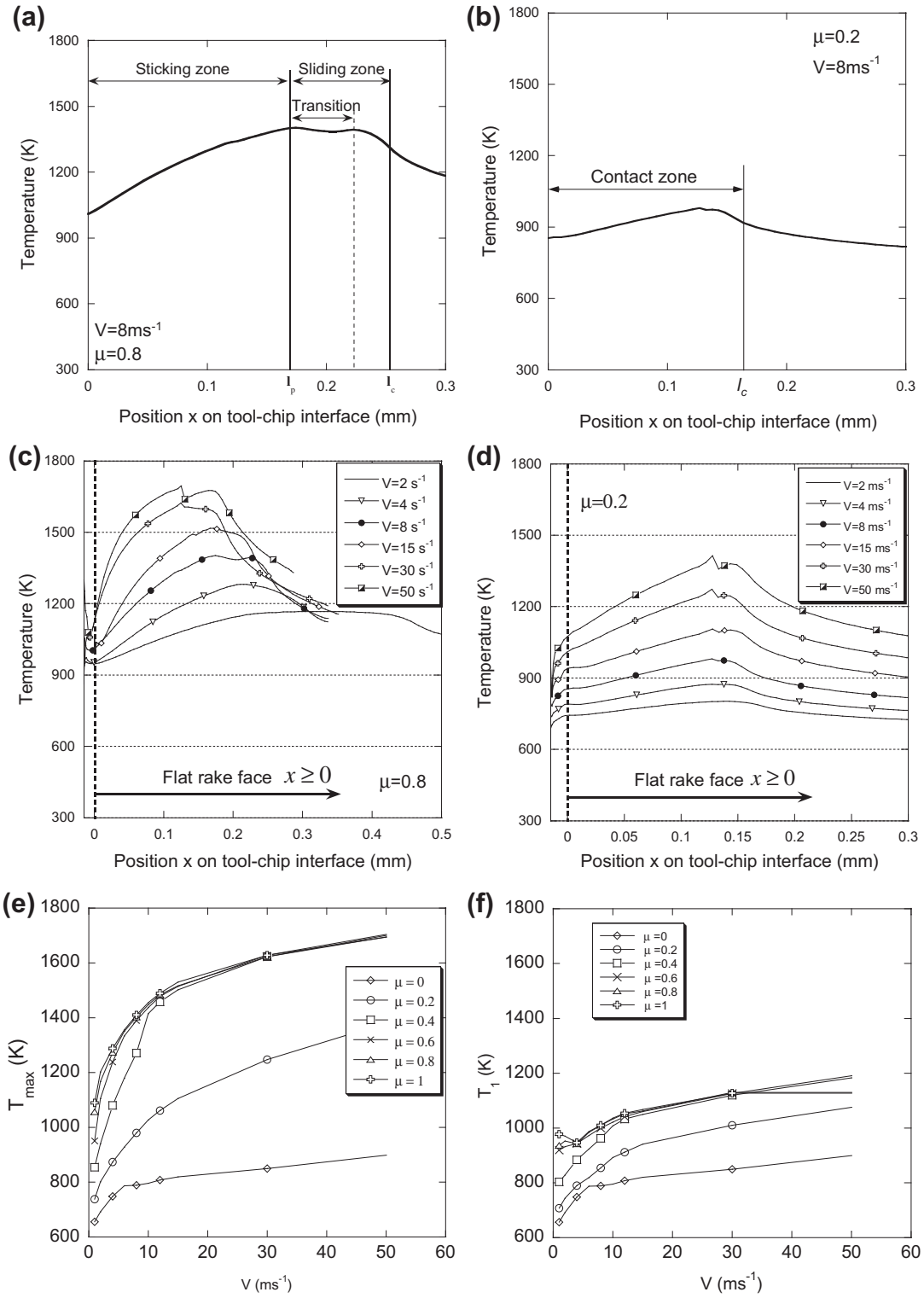

Fig. 6. Chip temperature on the tool rake face ($x \geqslant 0$) for tests T4 of Table 3. (a) Same conditions as for Fig. 3, (b) same conditions as for Fig. 4, (c) effect of the cutting speed for $\mu = 0.8$, (d) effect of the cutting speed for $\mu = 0.2$, (e) evolution of T_{max}, the maximum chip temperature on the rake face, in terms of the cutting speed for various values of the sliding friction coefficient μ. For $\mu \leqslant 0.2$ the contact regime is always sliding. For $\mu \geqslant 0.4$ the contact appears to be dominated by the sticking regime when the cutting speed is increased. The transition from sliding friction to contact dominated by sticking is clearly seen for $\mu = 0.4$. The transition starts at the cutting speed $V = 8$ ms^{-1} and is fully accomplished at $V = 12$ ms^{-1}. Then, the value of T_{max} becomes independent of μ. (f) Evolution with respect to cutting speed of the temperature T_1 at the entry I of the tool rake face. It is worth noting that, when $\mu > 0.4$ (sticking dominated contact), the sensitivity of T_1 with respect to V is relatively weak compared to that of T_{max}.

(sticking zone) or frictional heating (sliding zone). The evolution of $T_{max} - T_1$ with V results from the balance between heat generation along the interface and heat transfer towards the tool and the chip. At low cutting speeds, cooling due to heat transfer is dominant and consequently $T_{max} - T_1$ is tending to zero.

The increasing of T_1 with V may be related to the phenomenon of plastic flow localization frequently observed in visco-plastic materials exhibiting thermal softening and subject to high strain rates. In the present machining problem, it is likely that plastic deformation is accumulated near the tool tip (a zone of stress

concentration) and that a localization process is activated at large cutting speeds. By increasing the cutting speed, the thickness of the localization zone is reduced while plastic deformations and temperature are augmented. This observation may explain the growth of the temperature T_1 with V. For a given cutting speed, T_1 is seen to be increasing with μ, Fig. 6f. This is in keeping with the fact that the localization process is more easily triggered for high friction since sticking is favored (the condition of zero sliding velocity promotes shear localization near the tool–chip interface). However, as seen in Fig. 6f, the values of T_1 becomes weakly dependent upon μ when contact is dominated by sticking i.e. for $\mu \geqslant 0.4$. In that case, T_1 appears to be only slightly sensitive to cutting speed.

4.3.1. Law governing the evolution of the chip temperature at the tool rake face

The dependence of $T_{\max} - T_1$ with respect to cutting conditions and material properties can be characterized by analytical means. It is assumed that the distribution of the shear stress along the tool rake face has the form:

$$\tau(x) = \tau_0 \left(1 - \frac{x}{l_c}\right)^{\xi_1} \tag{9}$$

The decay of τ with x is characterized by the exponent ξ_1. For small values of ξ_1 the stress profile is rather flat with a brutal drop to zero at the end of contact. For $\xi_1 > 1$ the stress profile is peaked at $x = 0$ and shows a smooth decay to zero at $x = l_c$. Therefore a large variety of stress profiles can be approached through relationship (9).The scaling factor τ_0 is related to the tangential component $F_t(rake)$ of the force exerted by the chip on the part IJ $(0 \leqslant x \leqslant l_c)$ of the tool rake face, see Fig. 2. By performing the integration of the shear forces along the contact zone, we have:

$$\tau_0 = \frac{F_{t(rake)}(\xi_1 + 1)}{l_c} \tag{10}$$

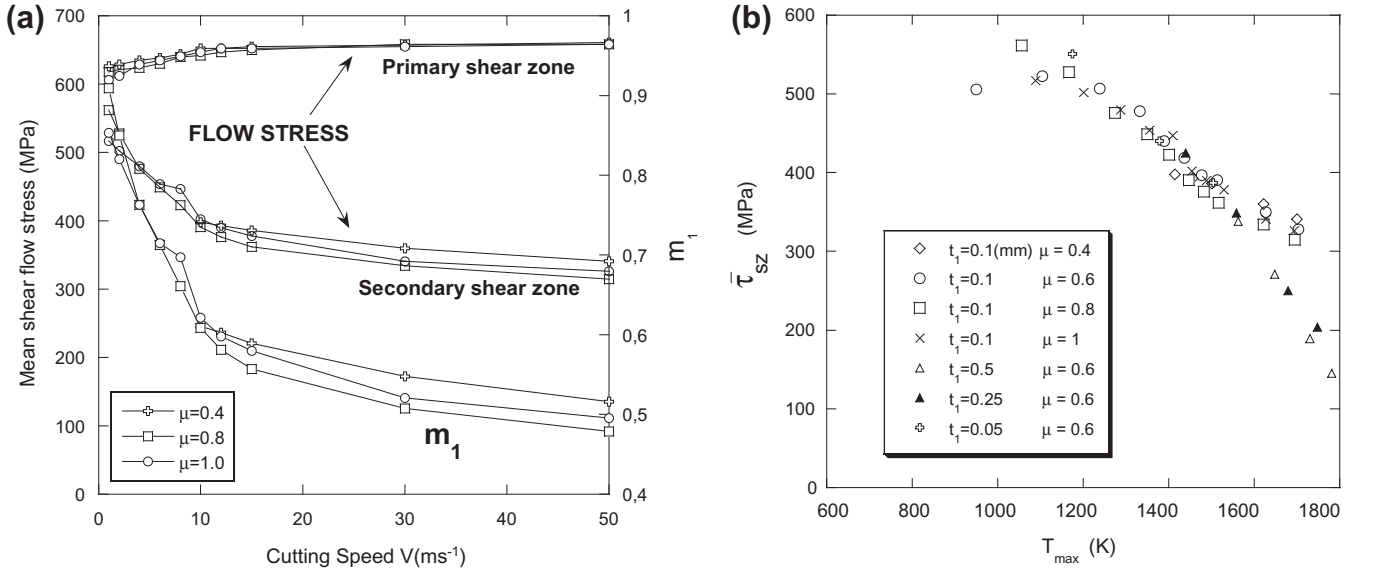

Fig. 7. (a) Evolution with respect to the cutting speed V of the mean flow stress $\bar{\tau}_{SZ}$ along the secondary shear zone (sticking zone) and of the mean flow stress $\bar{\tau}_{PZ}$ in the primary shear zone for tests T4 of Table 3. We consider values of the sliding friction coefficient $\mu \geqslant 0.4$, for which sticking contact becomes dominant when the cutting speed is increased. $\bar{\tau}_{SZ}$ decays significantly with V as an effect of thermal softening, while $\bar{\tau}_{PZ}$ appears to be weakly sensitive to V. The evolution of the ratio $m_1 = \bar{\tau}_{SZ}/\bar{\tau}_{PZ}$ is also reported (scaling on the right). (b) Correlation between $\bar{\tau}_{SZ}$ and $T_{\max}$ (maximum chip temperature on the rake face). All tests T4 of Table 3 ($t_1 = 0.1$ mm) for which sticking occurs ($l_p \neq 0$) are reported. For instance for $\mu = 0.8$ results are represented by ten square symbols since ten values of the cutting speed have been considered in the range $1 \leqslant V \leqslant 50$ ms^{-1}. Tests T6 corresponding to various values of the uncut chip thickness ($t_1 = 0.05$ mm, $t_1 = 0.25$ mm and $t_1 = 0.5$ mm) are also considered. The striking feature is that for the wide range of cutting speeds, sliding friction coefficients and feeds considered, the results appear to be more or less aligned along a single curve. This is a clear demonstration that the evolution of the mean shear flow stress $\bar{\tau}_{SZ}$ is mainly ruled by thermal softening. Strain hardening and strain rate sensitivity of the work material play a minor role for the work-material considered here.

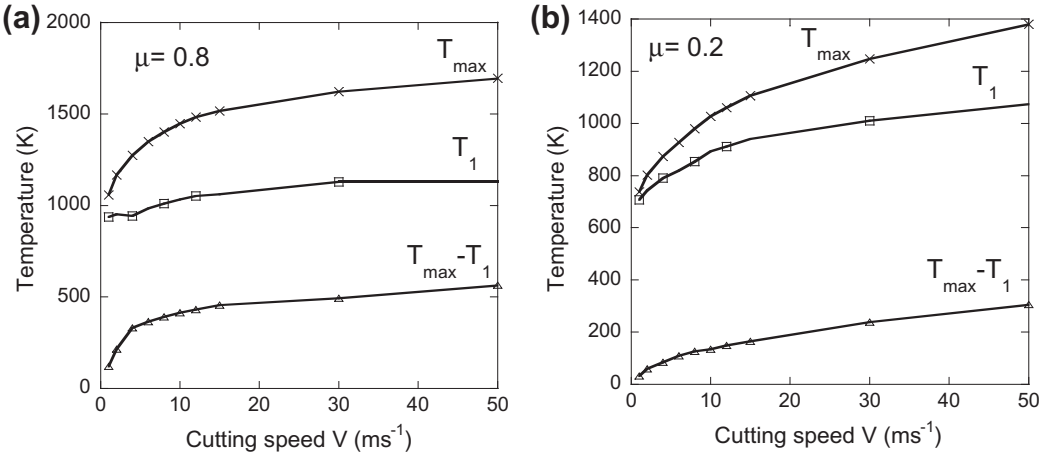

Fig. 8. Evolutions of the chip temperature on the tool–chip interface with respect to the cutting speed for (a) $\mu = 0.8$, (b) $\mu = 0.2$. $T_{\max}$ is the maximum temperature and T_1 is evaluated at I, see Fig. 2. Conditions correspond to tests T4 of Table 3.

Heat is mostly generated by plastic deformation within the bulk material (primary shear zone and secondary shear zone) and by friction along the sliding zone. In general, heat generation is negligible in the rest of the chip.

When sticking is absent, friction heating is distributed all along the tool–chip interface, the rate of heating per unit surface being given by:

$$Q = \tau V_c \tag{11}$$

where V_c is the chip velocity at the interface, and τ is the shear stress. If sticking occurs, it happens that the thickness of the secondary shear zone becomes very thin at high cutting speeds, see Section 5.1. In that case the heat source can be assumed to be localized at the tool–chip interface (the thickness of the secondary shear zone being neglected), and the relationship (11) holds all along the tool–chip interface (sticking and sliding zones). This simplified framework is adopted in the following.

The heat transfer problem associated to surface heating defined by (11) can be solved by using the Laplace transform technique as in Moufki et al. (1998). The temperature distribution along the tool–chip interface is found to be of the following form:

$$T(x) - T_1 = \eta_{eff} \frac{\tau_0 \sqrt{V_c l_c}}{\sqrt{\pi k \rho C_p}} G(x/l_c, \xi_1) \tag{12}$$

$$G\left(\frac{x}{l_c}, \xi_1\right) = \int_0^{x/l_c} \left(1 - \frac{x}{l_c} + u\right)^{\xi_1} \frac{1}{\sqrt{u}} du \tag{13}$$

In Eq.(12) η_{eff} is an effective coefficient of heat partition which accounts for the fact that, along the sticking zone, the totality of the heat is generated within the chip (secondary shear zone), while, along the sliding zone, only the fraction $\eta = 0.5$ of frictional heat is attributed to the chip.

Let us denote by $x_{\max}$ the position of the maximum chip temperature on the rake face. From (12) and (13), $x_{\max}/l_c$ and the maximum $G_{\max}$ of the function $G(x/l_c, \xi_1)$ are solely function of the stress exponent ξ_1. Thus, for given cutting conditions, we have:

$$T_{\max} - T_1 = \eta_{eff} \frac{\tau_0 \sqrt{V_c l_c}}{\sqrt{\pi k \rho C_p}} G_{\max}(\xi_1) \tag{14}$$

By using Eq. (10) it follows that:

$$T_{\max} - T_1 = K_1 \frac{\bar{\tau}}{\rho C_p} \sqrt{P_e} \tag{15}$$

with:

$$K_1 = \frac{1}{\sqrt{\pi}} \eta_{eff} (\xi_1 + 1) G_{\max}(\xi_1) \tag{16}$$

$$\bar{\tau} = \frac{F_t(rake)}{l_c} \tag{17}$$

$$P_e = \frac{V_c l_c}{(k/\rho C_p)} \tag{18}$$

$\bar{\tau}$ is the mean shear stress on the rake face ($0 \leqslant x \leqslant l_c$). From Eq. (15), $(T_{\max} - T_1)/T_0$ appears as the product of the square root of the Péclet number P_e (accounting for heat transfer) by the dimensionless number $\frac{\bar{\tau}}{\rho C_p T_0}$ that is related to heat production along the tool–chip interface by dissipation.

For $\mu \geqslant 0.4$, it will be shown that the dependence of $T_{\max} - T_1$ with respect to the cutting conditions V and t_1 can be well accounted for (in a certain range of these parameters) by a single calibration of the non-dimensional factor K_1 in Eq. (15). For small values of friction, K_1 is function of μ, in part because of the dependence of the stress distribution with respect to μ.

The evolution of $T_{\max} - T_1$ with the chip velocity V_c is analyzed in Fig. 9. The chip velocity is evaluated in terms of the cutting speed V according to the relationship (B1) of Appendix B, with values of the shear angle given by $\phi = \arctan(t_1/t_2)$. The chip thickness t_2 (see Fig. 2) is evaluated numerically.

In Fig. 9a numerical results are compared against analytical results given by Eq. (15) (solid lines) by taking $K_1 = 0.336$ for $\mu = 0.2$ and $K_1 = 0.519$ for $\mu = 0.8$. Numerical estimates of $F_t(rake)$ and of the contact length l_c are used to calculate $\bar{\tau}$ and the Peclet number in Eq.(15). It is worth noting that, by using the same value $K_1 = 0.519$, results of similar quality can be obtained for all friction coefficients such that $\mu \geqslant 0.4$ (see Fig. 9c for $\mu = 0.4$). This is related to the fact that, for $\mu \geqslant 0.4$, the contact regime is mostly controlled by sticking. The correlation between numerical results and those predicted by Eq. (15) is generally good but is less accurate at small velocities as shown in the loglog diagram displayed in Fig. 9b. For $\mu = 0.8$, this discrepancy may be attributed to the fact that the secondary shear zone is getting thicker at small velocities, see Section 5.1. Thus, the hypothesis used to derive Eq. (15), that heat is mostly dissipated nearby the tool face, is losing validity. Another source of divergence comes from the assumption made in the analytical approach that heat conduction effects are negligible in the direction tangential to the tool–chip interface, see Moufki et al. (1998). This assumption is only suitable when the chip velocity is sufficiently large.

The important variation of the coefficient K_1 when considering low friction ($\mu = 0.2$) and high friction ($\mu = 0.8$) can be related, as mentioned earlier, to the nature of the mechanisms of heat dissipation nearby the tool–chip interface. For low friction, the heating is due to friction. The heat source is located at the interface and is partitioned as 50% allocated to the chip and 50% to the tool, according to the value $\eta = 0.5$ that was entered in the Finite Element calculations. For $\mu = 0.8$, sticking contact is dominant, and the heat source is now located in the secondary shear zone. Therefore, with the low value 2000 W m^{-2} K^{-1} of the interface thermal conductance, about 100% of the heating is likely to be attributed to the chip. This is why the value of K_1 for $\mu = 0.8$ is larger than for $\mu = 0.2$.

4.3.2. Rate dependence of $T_{\max} - T_1$

It will be shown that the dependence of $T_{\max} - T_1$ with respect to the chip velocity can be described in terms of a power law $T_{\max} - T_1 \propto (V_c)^{\alpha}$. The exponent α depends on the nature of contact (pure sliding or sticking dominated contact) and is constant in a certain range of velocities.

For $\mu = 0.2$ the dependence of $T_{\max} - T_1$ with respect to the chip velocity is represented by a straight line of slope 0.5 in the log–log diagram of Fig. 9b. Thus, $T_{\max} - T_1$ is scaled by $\sqrt{V_c}$. It should be noted that for $\mu = 0.2$, $F_t(rake)$ and l_c appear from numerical calculations to be weakly dependent upon velocity. Then, Eqs. (17), (18) and (15) imply $T_{\max} - T_1$ to be scaled by $\sqrt{V_c}$. This result is not affected by the value of K_1. Indeed, in Fig. 9b the level of the solid lines is controlled by K_1 but the slope is not influenced by this factor.

For $\mu = 0.8$ (high friction) analytical and numerical results are seen in Fig. 9b to be well correlated for sliding velocities larger than $V_c = 1.25$ ms^{-1} (cutting velocities $V \geqslant 4$ ms^{-1}). The variation of $T_{\max} - T_1$ with respect to the chip velocity V_c is represented by a straight line with slope 0.2 (regime *II*). A larger slope is found at lower velocities (regime *I*). The transition between the two regimes occurs at the chip velocity $V_c = 1.25$ ms^{-1} (cutting speed $V = 4$ ms^{-1}). It is interesting to observe in Table 4 of Molinari et al. (2011) that for increasing cutting velocities the sticking ratio l_p/l_c sustains a rapid growth during regime *I*, while a saturation of l_p/l_c is found in regime *II*. For regime *II*, the contact appears to be dominated by sticking. Since the secondary shear zone takes the

appearance of a thin boundary layer at large cutting speeds, the hypothesis that heat generation is localized in a close vicinity of the tool face is satisfied. This explains the good correspondence between numerical results and Eq. (15) for regime *II*.

The results shown in Fig. 9c are relative to $\mu = 0.4$. This case is of special interest, as a clear transition from sliding friction to dominant sticking was observed in Fig. 6e. As said before, the scaling factor in Eq. (15) is taken identical for all sliding friction coefficients verifying the condition $\mu \geqslant 0.4$ ($K_1 = 0.519$). Similarly to Fig. 9b, a regime *II* characterized by $T_{\max} - T_1 \propto (V_c)^{0.2}$ can be observed at large velocities in the loglog diagram of Fig. 9d. The transition to regime *II* occurs at the cutting speed $V = 8$ ms^{-1} (chip velocity $V_c = 3.23$ ms^{-1}) and corresponds almost to the saturation of l_p/l_c, see Table 4 of Molinari et al. (2011). As for $\mu = 0.8$, sticking contact turns out to be dominant in regime *II*. For regime *I*, we nearly have $T_{\max} - T_1 \propto (V_c)^{0.5}$, see Fig. 9d; contact is dominated by sliding. The velocity exponent 0.5 is consistent with the result found in Fig. 9b for the value $\mu = 0.2$ of the sliding friction coefficient for which pure sliding occurs. The existence of two distinct contact regimes suggests that two values of K_1 may be used in Eq. (15) according to whether we are below or above the transition velocity between regimes *I* and *II*. So doing, a better correspondence between numerical predictions and Eq. (15) would be obtained for the whole range of cutting velocities (results not shown).

The cutting speed corresponding to the transition to regime *II* is a decreasing function of μ. For $\mu = 0.4$ it was found to be about $V = 8$ ms^{-1} (chip velocity $V_c = 3.23$ ms^{-1}), for $\mu = 0.6$ it has the value $V = 4$ ms^{-1} ($V_c = 1.35$ ms^{-1}). For larger friction the transition velocity becomes almost independent of μ. Thus, for $\mu = 0.8$ transition occurred at $V = 4$ ms^{-1} ($V_c = 1.25$ ms^{-1}) as for $\mu = 0.6$.

4.3.3. Effect of feed and tool edge radius on chip temperature at the rake face

Values of $T_{\max}$, T_1 and $T_{\max} - T_1$ are reported in Fig. 10a in terms of the cutting speed for various feeds ($t_1 = 0.05$ mm, $t_1 = 0.1$ mm, $t_1 = 0.25$ mm and $t_1 = 0.5$ mm) and for $\mu = 0.6$. These numerical data are related to the tests T4 and T6 of Table 3. For a given cutting speed, it appears that $T_{\max}$, T_1 and $T_{\max} - T_1$ are increasing functions of t_1. However, for large feeds, T_1 becomes weakly sensitive to t_1 and $T_{\max} - T_1$ is weakly sensitive to the cutting speed for $V \geqslant 8$ ms^{-1}.

Eq. (15) shows the importance of the Péclet number, P_e, in the evolution of $T_{\max} - T_1$. Considering that the contact length l_c is scaled by the feed t_1, it is natural to investigate the relationship between chip temperature and cutting conditions through the dimensionless cutting speed $\bar{V} = Vt_1/a$, with $a = \frac{k}{\rho C_p}$ being the thermal diffusivity of the work-material. It is worth noting that $\bar{V}$ depends on the control parameters V and t_1 (cutting conditions) while P_e is function of the dependent variables V_c and l_c (resp. chip velocity and contact length). Fig. 10b shows the variation of $T_{\max}$ with respect to $\bar{V}$. For all values of the feed considered, the results appear to be grouped along a well defined master curve. Similar results are obtained for T_1 in Fig. 10b. These results show that, for high values of the sliding friction coefficient, the cutting process is essentially controlled by heat transfer through the dimensionless number $\bar{V}$.

Fig. 11 illustrates for $\mu = 0.8$ the effect of the tool edge radius ($R = 0.015$ mm and $R = 0.030$ mm) on $T_{\max}$ and T_1. The uncut chip thickness is $t_1 = 0.1$ mm. Data correspond to tests T4 and T5 of Table 3. It is seen that the temperature T_1 near the tool edge is increasing with R, while the effect of R seems to be negligible on $T_{\max}$.

4.4. Hot spot position

The position $x_{\max}$ of the maximum chip-temperature on the rake face is an interesting feature that can be assessed by experimental measurements, Sutter et al. (2003), Sutter and Ranc (2007). From the relationship (12) it was deduced that $x_{\max}/l_c$ is solely function of the shear stress exponent ξ_1. It is seen in Fig. 12 that $x_{\max}/l_c$ is a decreasing function of ξ_1. These results were obtained by seeking numerically the position $x_{\max}$ of the maximum of the function $\hat{x} \to G(\hat{x}, \xi_1)$ defined by relationship (13). Results can be derived analytically if ξ_1 is an integer, see Moufki et al. (1998). In particular it can be verified by direct integration that $x_{\max}/l_c = 1$ for $\xi_1 = 0$ and $x_{\max}/l_c = 0.5$ for $\xi_1 = 1$. From Fig. 12, it results that the position of the temperature maximum is getting closer to the end of the tool–chip contact ($x = l_c$) when the shear stress profile becomes more flat (small ξ_1).

Finite Element results showing $x_{\max}/l_c$ versus cutting speed V are displayed in Fig. 13a for $\mu = 0.2$ and $\mu = 0.8$. Test conditions are those reported as T4 in Table 3. The value of $x_{\max}/l_c$ turns out to be weakly sensitive to the cutting speed and to be in the range 0.65–0.8. $x_{\max}/l_c$ is larger (about 0.8) for low friction $\mu = 0.2$. The later result can be correlated to the shear stress profile reported in Fig. 4b. The stress exponent associated to $V = 8$ ms^{-1} and $\mu = 0.2$ is found to be $\xi_1 = 0.23$. The corresponding prediction of the analytical approach is $(x_{\max}/l_c)_{analytic} = 0.86$, see Fig. 12, a result in close agreement with the numerical prediction (about 0.8) displayed in Fig. 13a. For $\mu = 0.8$, we have $\xi_1 = 0.4$. The analytical approach provides $(x_{\max}/l_c)_{\text{analytic}} = 0.75$, see Fig. 12. This value is below those obtained for $\mu = 0.2$ in agreement with FE results presented in Fig. 13a.

The evolution of $x_{\max}/t_1$ in terms of V is shown in Fig. 13b. For $\mu = 0.2$ it is observed that $x_{\max}/t_1$ is nearly insensitive to the cutting speed in the range of velocities considered here. However, for $\mu = 0.8$ a rapid decreasing of $x_{\max}/t_1$ is seen until the asymptotic value of about 1.1 is reached at $V > 25$ ms^{-1}. This trend towards an asymptotic value is related to the transition to a contact dominated by sticking, as discussed previously.

The evolution of $x_{\max}/l_p$ in terms of the cutting speed is displayed in Fig. 13c for $\mu = 0.8$. Such representation has no meaning for low values of μ since $l_p = 0$ in that case. Fig. 13c reveals that the position of the temperature maximum is located at the exit of the sticking zone for $V > 4$ ms^{-1}. In this velocity range we note also in Fig. 13c a saturation of the ratio l_p/l_c corresponding to the transition to a contact regime dominated by sticking.

4.5. Effect of thermal properties of the tool–chip interface

The thermal properties of the tool–chip interface are characterized by the thermal conductance κ and the coefficient η of partition of the frictional energy (along the sliding zone). The value $\eta = 0.5$ was adopted. Along the sticking zone, the temperature is insensitive to the value of η, since the frictional energy vanishes (the sliding velocity is equal to zero).

The value of the thermal conductance used so far was $\kappa = 2000$ W m^{-2} K^{-1}. Few experimental characterizations of κ can be found in the literature for situations relevant to machining (high pressure, high sliding velocities). Of note are the experiments recently conducted by Brocail et al. (2010) coupled with a method for deriving the thermal conductance of the tool–chip interface, Guillot et al. (2008). In Brocail et al. (2010), a tribometer was developed which is able to reach high pressure of the order of 1 GPa. The system was composed of a tool made up of an AISI M2 steel rubbing on AISI 1045 or on AISI 304L steels. A value of about $\kappa = 10^4$ W m^{-2} K^{-1} was found in these experiments.

In order to quantify the effect of the thermal conductance of the tool–chip interface, two quite different values have been considered: $\kappa = 2000$ W m^{-2} K^{-1} (low conductance) and $\kappa = 10^9$ W m^{-2} K^{-1} (high conductance). Calculations are conducted under conditions K of Table 3. It must be noted that these results are obtained for a mean mesh size of 2 μm (while most of the other results of the paper are relative to a mean mesh size of 4 μm). This allowed us to make a mesh sensitivity analysis. Most of the results appeared to be nearly insensitive to the decreasing of the mesh

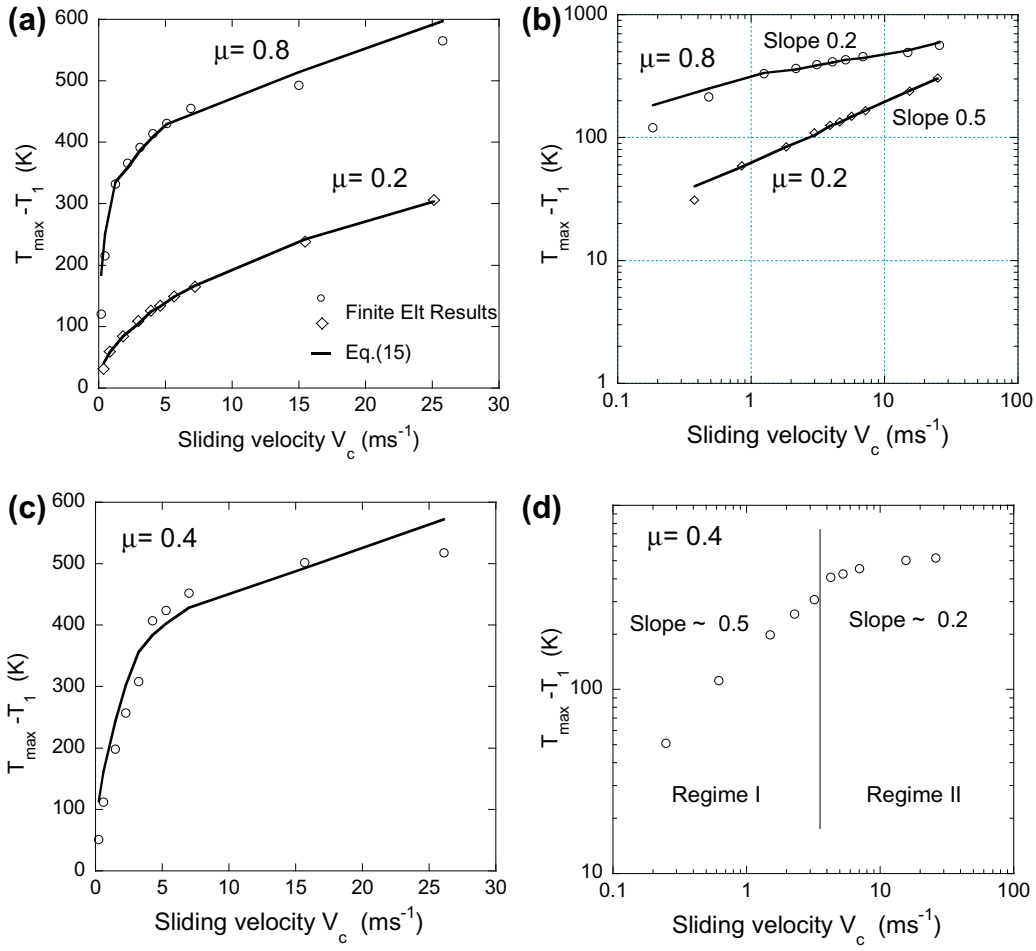

Fig. 9. Variation of $T_{max} - T_1$ in terms of the chip velocity V_c. $T_{max} - T_1$ represents the growth of the chip temperature on the tool rake face between *I* (Fig. 2) and the hot spot. Conditions correspond to tests T4 of Table 3. (a) Numerical calculations (circles for $\mu = 0.8$, diamonds for $\mu = 0.2$) are compared to predictions based on Eq. (15) (solid curves), (b) same results displayed in a loglog-diagram, (c) $\mu = 0.4$, (d) Numerical results (circles) for $\mu = 0.4$ presented in a loglog-diagram. Two contact regimes can be distinguished. Regime *I*, that occurs at low chip velocities $V_c < 3.23$ ms^{-1} (cutting speed $V < 8$ ms^{-1}), is dominated by sliding friction. Regime *II* is dominated by sticking contact and takes place for $V_c > 3.23$ ms^{-1}. Note that $T_{max} - T_1$ is scaled as $(V_c)^{0.5}$ for regime *I*. The same velocity exponent *0.5* was found in (b) in the case of low friction $\mu = 0.2$ where pure sliding occurred. For regime *II*, we have $T_{max} - T_1 \propto (V_c)^{0.2}$ as for the high friction case $\mu = 0.8$ displayed in (b) for which contact was found to be dominated by sticking.

size. The maximum deviation was obtained for x_{max}/l_p (about 10%) but the trends (for instance the dependence of x_{max}/l_p upon cutting speed) were found to be very similar. Therefore, it was justified to work with the mesh size of 4 μm which permitted to save computational time.

The evolution of T_{max} in terms of the cutting speed is reported in Fig. 14a for $\kappa = 2000$ W m^{-2} K^{-1} and $\kappa = 10^9$ W m^{-2} K^{-1}. The results reveal a weak dependence of the chip temperature with respect to κ. For $\kappa = 10^9$ W m^{-2} K^{-1} the chip and the tool temperatures have same values since the thermal resistance of the interface is negligible. However, for $\kappa = 2000$ W m^{-2} K^{-1} the temperature is discontinuous across the interface (results not shown for the tool temperature).

Fig. 14b displays the variation of x_{max}/l_c with the cutting speed. An increasing of about 10% is found when changing the thermal conductance from $\kappa = 2000$ W m^{-2} K^{-1} to $\kappa = 10^9$ W m^{-2} K^{-1}. However, the trends are conserved as the velocity dependence happens to be rather weak in both cases. Therefore, as far as the chip temperature is concerned, it is enough to analyze the results related to the value $\kappa = 2000$ W m^{-2} K^{-1}.

4.6. Comparison with experimental data

Chip temperatures have been measured by Sutter et al. (2003) and Sutter and Ranc (2007) for a medium carbon steel (42CrMo4) and a low carbon steel C15 by using a CCD camera in the visible range. The maximum of the chip temperature T_{max} is function of the feed and cutting speed. Measurements were done for the C15 steel at high cutting speeds (from 20 ms^{-1} to 60 ms^{-1}) by using a ballistic set-up, Sutter et al. (1998). Two values of the uncut chip thickness were tested: $t_1 = 0.25$ mm and $t_1 = 0.5$ mm. Maximum temperatures were observed for the C15 steel in the range from 920 K to 1020 K. For the 42CrMo4 steel, the maximum temperature was found for $t_1 = 0.5$ mm to be 1100 K at $V = 20$ ms^{-1}. An important difference exists with respect to $T_{max} = 1730$ K obtained in the present modeling. However, it must be reminded that the quasi-stationary states considered in our theoretical approach are reached for times of the order of 1000 μs, while in the ballistic experiments of Sutter and Ranc (2007), Sutter et al. (2003), the time duration of the cutting process is very short (of the order of 100 μs) so that the cutting process is likely to be in a transient regime. Another source of discrepancy might be related to the constitutive response of the steels considered in experiments and to friction characteristics.

It is probably more justified to discuss trends. In the range of cutting velocities 20 ms^{-1} $\leqslant V \leqslant$ 60 ms^{-1} the increasing of the maximum temperature was measured by Sutter and Ranc (2007) to be about 50 K when changing the feed from $t_1 = 0.25$ mm to $t_1 = 0.5$ mm. In the present calculations the increasing of the maximum temperature is 55 K at $V = 20$ ms^{-1} and 42 K at $V = 40$ ms^{-1},

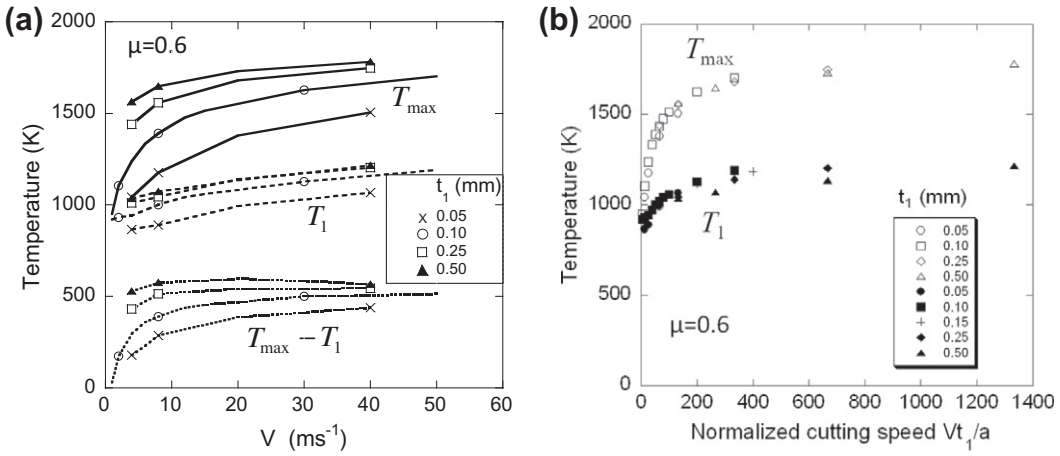

Fig. 10. (a) Evolutions of the chip temperatures T_{max}, T_1 and of $T_{max} - T_1$ with respect to the cutting speed for various values of the uncut chip thickness t_1. Conditions are those related to tests T4 with $\mu = 0.6$ and tests T6 of Table 3, (b) evolution of temperature in terms of the normalized cutting speed $\bar{V} = Vt_1/a$, with a being the thermal diffusivity of the work-material. Results are grouped along two master curves, respectively for T_{max} and T_1. For the values 0.05, 0.25, 0.50 mm of the feed, four cutting speeds are considered $V = 4, 8, 20, 40$ ms^{-1}. For $t_1 = 0.10$ mm the cutting speed spans from 1 to 50 ms^{-1}. For T_1, the additional feed 0.15 mm is taken into account.

see Fig. 10a. For the feeds $t_1 = 0.25$ mm and $t_1 = 0.5$ mm, the increasing of the temperature when the cutting speed was augmented from $V = 20$ ms^{-1} to $V = 60$ ms^{-1} was measured by Sutter and Ranc (2007) to be around 70 K. When extrapolating the curves of Fig. 10a to larger velocities the increasing of temperature can be estimated at about 75 K for the feed $t_1 = 0.25$ mm and 60 K for $t_1 = 0.5$ mm. Therefore, at high cutting speeds, both calculations and experiments indicate a rather weak dependence of the temperature with respect to the cutting speed.

Numerical results concerning the position of the hot spot are also compatible with experimental observations of Sutter and Ranc (2007). These authors found, for the C15 steel (low carbon) that x_{max}/t_1 was weakly sensitive to the cutting speed for $V > 20$ ms^{-1}. The experimental value of x_{max}/t_1 was about 0.85 in average. This value is smaller than 1–1.2 obtained numerically. The gap may be related to differences between the thermo-mechanical responses of respectively the C15 steel used in experiments and the medium carbon steel 42CrMo4 analyzed in the modeling. But we are more interested by trends (e.g. variation of x_{max}/t_1 with cutting speed) than by the magnitude of the quantities studied.

Overall, the whole set of experimental trends reported by Sutter and Ranc (2007) was found to be in good correlation with the present numerical results.

5. Morphology of the secondary shear zone and boundary layer effects

Sticking of the chip to the tool occurs along the segment II' ($0 \leqslant x \leqslant l_p$), see Fig. 15. Along the sticking zone, the chip undergoes intense plastic shearing within the so called secondary shear zone characterized by the length l_p (x-direction) and the thickness l_2 measured in the y-direction (orthogonal to the rake face). The dependence of these morphological characteristics upon μ and cutting conditions is analyzed in the following.

5.1. Thickness of the secondary shear zone

The thickness $l_2(x)$ varies with the position x along the rake face. Using a fine mesh (2 μm), l_2 has been characterized at the point S indicated in Fig. 15 by applying the following methodology. The distribution of the equivalent strain rate was considered on the line SS' aligned with the free surface of the workpiece and orthogonal to the rake face at S. The maximum of the Mises-equivalent strain rate $\dot{\varepsilon}_{eq}^{max}$ was observed to be at S. The thickness of the shear zone at S was evaluated as $l_2(S) = SS_1$ with S_1 being the point of SS' where the equivalent strain rate is equal to $\dot{\varepsilon}_{eq}^{max}/10$. This characterization of

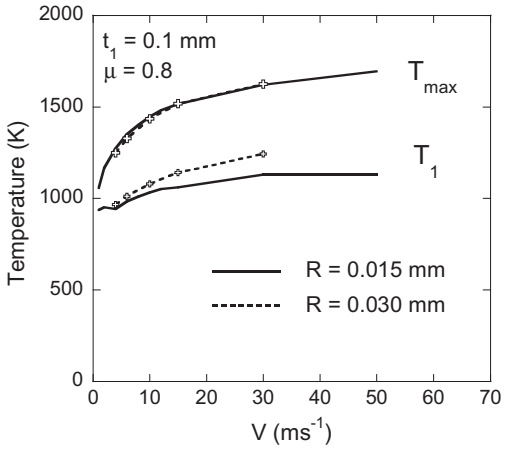

Fig. 11. Effect of the cutting edge radius on T_{max} and T_1. Conditions are those of tests T4 with $\mu = 0.8$ and tests T5 of Table 3.

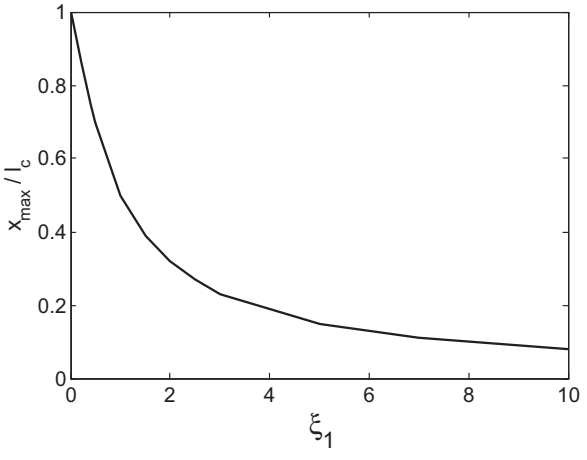

Fig. 12. Dependence of x_{max}/l_c with respect to the shear stress exponent ξ_1. x_{max} is the position of the hot spot (chip maximum temperature) on the rake face.

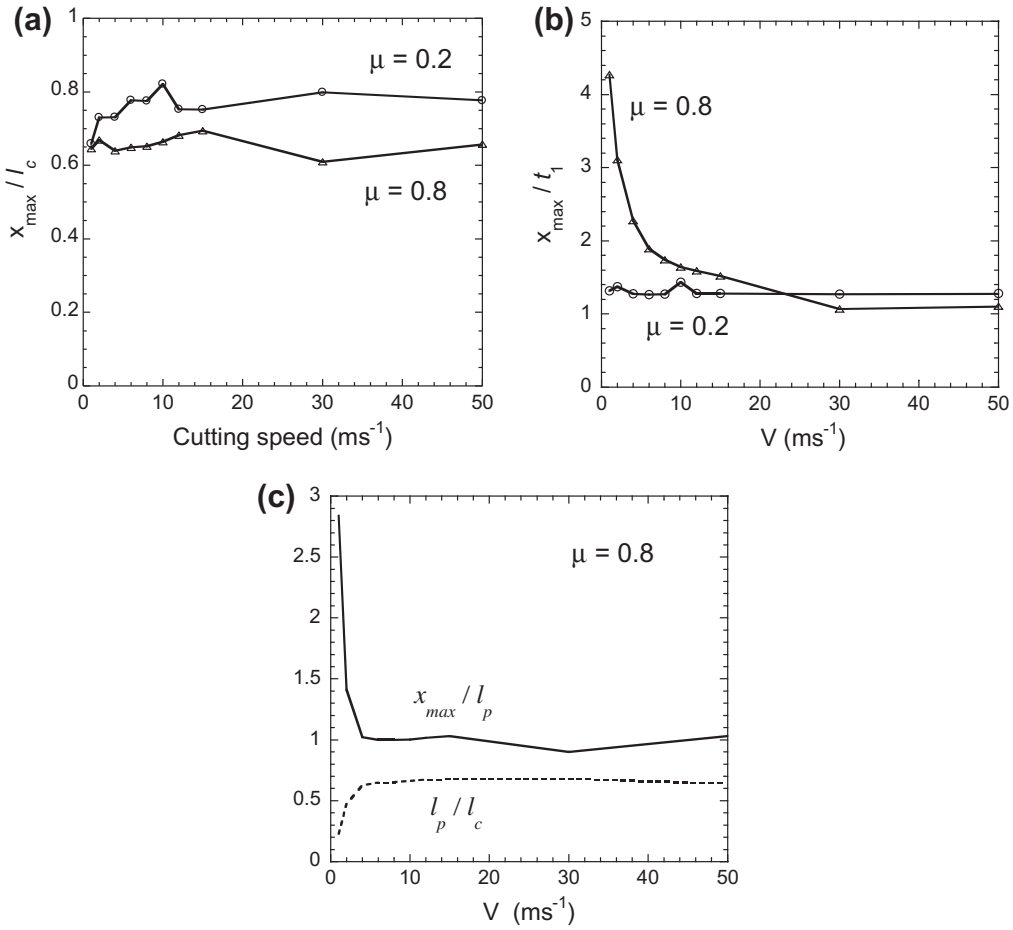

Fig. 13. Position of the hot spot, x_{max}, on the rake face versus cutting speed. Test conditions are those reported as T4 in Table 3. Two values of friction are considered, $\mu = 0.2$ and $\mu = 0.8$: (a) x_{max}/l_c, (b) x_{max}/t_1, (c) x_{max}/l_p and l_p/l_c.

the local value of the secondary shear zone width is somewhat arbitrary but is enough for the purpose of delineating trends. Fig. 16a and b display the evolution of the thickness $l_2(S)$ in terms of respectively the cutting speed and a local measure of the chip velocity. The local chip velocity was defined as the x-component of the particle velocity at the point S' which is at the distance $t_2/2$ from S, see Fig. 15. Test conditions refer to T4 in Table 3. Three values of the sliding friction coefficient were considered ($\mu = 0.4, 0.6, 0.8$). The width of the secondary shear zone $l_2(S)$ happens to decrease rapidly from about 65 μm to 4 μm when the cutting speed varies from $V = 1$ ms^{-1} to $V = 20$ ms^{-1}.

An interesting analogy can be drawn between the evolution of the secondary shear zone at high cutting speeds and the process of adiabatic shearing occurring in metals subject to rapid deformations. Adiabatic shear bands (ASB) are narrow lines with thickness of some micro-meters where intense shear deformation and high temperatures are localized, Bai and Dodd (1992), Tresca (1878). They frequently appear in metals as the result of a thermomechanical instability driven by thermal softening, Zener and Hollomon (1944), Recht (1964), Molinari and Clifton (1983), Wright (2002), Bonnet-Lebouvier et al. (2002). For fast processes and large deformations, the stabilizing effects of heat conductivity, strain hardening and strain rate hardening can be overcome by the destabilizing effect of thermal softening. If the characteristic time of the process is very small, there is no enough time for the heat generated by plastic deformation to be transferred outside the localization zone. This is the reason why flow instability turns out to be stronger for higher loading rate. Accordingly, the deformation is more localized at higher loading rates. As a matter of fact, ASB in metallic targets impacted by projectiles are observed to be thinner at higher impact velocities. Similarly, the width of ASB obtained when machining titanium or steels at high cutting speeds V is reduced by increasing V, Molinari et al. (2002). It was theoretically predicted by Wright and Ockendon (1992) and Dinzart and Molinari (1998) for material with linear thermal softening ($m = 1$ in the constitutive law (1)), that the thickness of an ASB is scaled by $1/V_{shear}$. Here, V_{shear} is the shear velocity (i.e. the variation across the shear band of the tangential component of the particle velocity). Some similitude can be seen between the secondary shear zone observed near the tool tip at high cutting speeds and the phenomenon of adiabatic shear banding. In both cases the material sustains an intense plastic shearing within a narrow band, the temperature is coupled to plastic strain, thermal diffusion and thermal softening play eminent roles. Also, the particle velocities within the shear zones have same direction as the shear velocity (this is not the case for the primary shear zone).

Following this analogy, the thickness $l_2(S)$ of the secondary shear zone at S should be scaled as $1/V_c$ according to Wright and Ockendon (1992) and Dinzart and Molinari (1998). In the present problem, the shear velocity is assimilated to the local chip velocity V_c at S', Fig. 15. The loglog diagram of Fig. 16c reveals that the scaling of l_2 by $1/V_c$ is satisfied. This finding is an indication that, at large cutting velocities, the secondary shear zone has same characteristics than an adiabatic shear band in which shear flow is controlled by the interplay of thermal softening, strain rate sensitivity and heat conduction effects (Actually, "adiabatic" appears to be a misleading denomination, as heat conduction effects have a significant role in structuring the shear flow within the band; however this denomination is commonly used in the

literature). For a given chip velocity, there is no clear dependence of l_2 upon the value of the friction coefficient (for $0.4 \leqslant \mu \leqslant 1$), see Fig. 16b and c. This is in line with the existence of a contact dominated by sticking. In that case, contact variables are solely controlled by the shear flow stress $\bar{\tau}_{SZ}$, with a weak dependence upon μ, see Figs. 6e and 7a.

For high cutting speeds, the secondary shear zone becomes so thin (few micro-meters), see Fig. 16a, that it behaves as a boundary layer with high localized heating and velocity gradient.

It must be noted that the scaling of the thickness of the boundary layer as $1/V_c$ is certainly doubtful when reaching extremely small dimensions, i.e. at very large sliding velocities. Then, nonlocal effects of the material response (e.g. gradient plasticity) would have a role to play and the thickness of the boundary layer would be controlled by the interplay between thermal effects and the nonlocal response of the material. Similar higher order gradient effects were discussed in the context of plastic shock waves and the analysis of the shock front, Molinari and Ravichandran (2006).

A comprehensive analysis of boundary layers resulting from the process of flow localization in thermal softening viscoplastic materials can be found in Gioia and Ortiz (1996).

5.2. Sticking length

The extension of the secondary shear zone along the tool rake face is characterized by the sticking length l_p. The dependence of l_p with respect to the sliding friction coefficient, the cutting conditions and the contact length are analyzed numerically and by analytical means. A special attention is accorded to the transition towards a contact regime dominated by sticking.

The evolution of l_p with respect to the cutting speed is shown in Fig. 17a for various values of the sliding friction coefficient μ. Cutting conditions are those related to tests T4 in Table 3. For low values of friction ($\mu \leqslant 0.2$), the chip is sliding along the tool for all values of the cutting speed considered here. For $\mu = 0.4$ the contact is entirely ruled by sliding ($l_p = 0$) for cutting velocities V below the transition velocity $V_{tr} = 8\ \mathrm{ms}^{-1}$. For $V > V_{tr}$ an abrupt change to a sticking mode is observed which is characterized by a sharp increase of l_p. V_{tr} is a decreasing function of μ. For a given value of μ, the transition from a pure sliding regime to a sticking mode is a consequence of the increasing of the interface temperature with cutting speed. The resulting drop of the flow stress of the workmaterial (thermal softening) favors tool–chip sticking. For large values of μ sticking is easier, therefore the transition velocity V_{tr} is smaller. The ratio l_p/l_c indicates which proportion of the contact zone is ruled by sticking. According to Fig. 17b, about 60–70% of the contact is governed by sticking above the transition velocity V_{tr}. Since the level of stresses is smaller in the sliding zone, it can be concluded that the overall contact forces (and therefore overall friction characteristics) are mostly controlled by sticking. It is worth observing in Fig. 17a and b that, for large friction ($\mu \geqslant 0.4$), l_p and l_p/l_c are tending to a saturation value which is weakly sensitive to the value of μ, as previously observed in Fig. 6e for $T_{\max}$ and in Fig. 7a for $\bar{\tau}_{SZ}$. It can be also noted that sticking is favored by larger values of μ. Therefore l_p and l_p/l_c are increasing with μ. This effect is important at low sliding velocities but is less significant at high cutting speeds. The tendency to a saturation regime will be further discussed in Section 6.

For a given test, let us assume that the normal stress distribution along the tool–chip interface is described by the relationship:

$$\sigma(x) = \sigma_0 \left(1 - \frac{x}{l_c}\right)^{\xi} \tag{19}$$

According to the Coulomb friction law, the shear stress distribution along the sliding zone has the form:

$$\tau(x) = \mu\sigma_0 \left(1 - \frac{x}{l_c}\right)^{\xi} \tag{20}$$

The limit $x = l_p$ between sticking and sliding zones is characterized by $\tau(l_p) = \tau_Y(l_p)$ where $\tau_Y(l_p)$ is the shear flow stress at $x = l_p$. At first approximation we shall consider that $\tau_Y(l_p)$ is given by the mean shear flow stress along the sticking zone. Then, the sticking length l_p appears to be of the form, see Ozlu et al. (2010):

$$l_p/l_c = 1 - \left(\frac{\bar{\tau}_{SZ}}{\mu\sigma_0}\right)^{1/\xi} \tag{21}$$

Fig. 17c shows for $\mu = 0.6$ the evolution of l_p/l_c with respect to the cutting speed. Testing conditions are again those of T4 in Table 3. We have compared numerical predictions of l_p/l_c with those of Eq. (21) using the values of $\bar{\tau}_{SZ}$ calculated numerically. The stress exponent was taken as $\xi = 0.23$ and for each test the value of σ_0 was scaled in order to have the best fit with the numerical stress distribution along the sliding zone. For instance, for the tests corresponding to the cutting velocities V = 2, 4, 6, 10, 12, 15, 30 ms^{-1} we had σ_0 = 950, 1000, 1150, 1100, 1000, 1000,1000 MPa. The trends predicted by Eq. (21) are in good correlation with numerical data. In particular, the transition towards a contact dominated by sticking is found to be at the cutting speed $V = 4\ \mathrm{ms}^{-1}$. This transition is mostly controlled by the thermal softening of the mean flow stress $\bar{\tau}_{SZ}$.

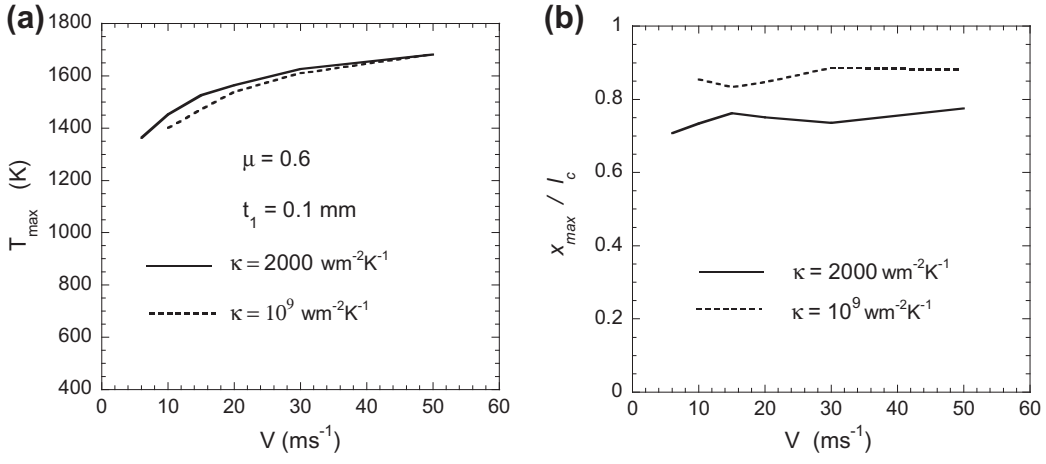

Fig. 14. Effect of the thermal conductance, κ, of the tool–chip interface. Calculations are conducted under conditions K of Table 3. Low and large values of κ are considered: $\kappa = 2000\ \mathrm{W\,m^{-2}\,K^{-1}}$ and $\kappa = 10^9\ \mathrm{W\,m^{-2}\,K^{-1}}$. Note that the mesh size is about 2 μm while most of the results of the paper are obtained with a mean mesh size of 4 μm. (a) $T_{\max}$ and (b) $x_{\max}/l_c$.

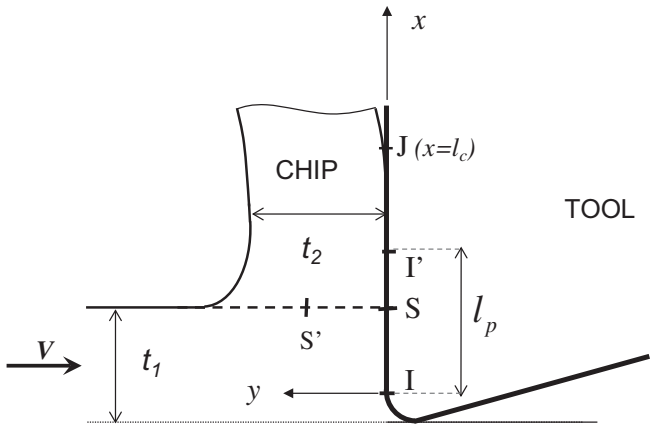

Fig. 15. Geometrical features used for the characterization of the morphology of the secondary shear zone.

It should be emphasized that the sticking length appears in the present approach as an outcome of the calculation while it is not so in several numerical approaches of the literature. For instance, Kountanya et al. (2009) used the Deform 2D software to simulate the chip formation for a 100Cr6 steel. The Zvorev model was implemented in this software, but the sticking length l_p had to be chosen a priori. As we have shown, the sticking length depends strongly on the sliding friction coefficient, but is also function of the cutting conditions and of the work-material properties. Indeed, the results related to conditions T4 of Table 3 show that $l_p = 0$ for small friction while for $\mu \geqslant 0.6$ the ratio l_p/t_1 varies mostly in the range 1.2–3.54, depending on values of μ and of the cutting speed. Therefore any arbitrary definition of l_p seems to be questionable.

Recently, Bahi et al. (2011) have proposed an analytical–numerical hybrid model of sticking and sliding contact for perfectly sharp tools. The trends of this model are in agreement with the results predicted here.

6. Discussion of the effects of the cutting speed

The effects of the cutting speed on process variables are recapitulated in this section. The cases of low and high friction are analyzed separately.

6.1. Low friction ($\mu \leqslant 0.2$)

At a given feed, the effect of the cutting speed V can be summarized as follows. For low values of the friction coefficient ($\mu \leqslant 0.2$) the chip is sliding along the tool for the whole range of cutting speeds considered here ($1\ \mathrm{ms}^{-1} \leqslant V \leqslant 50\ \mathrm{ms}^{-1}$). For a fixed value of μ, the process parameters are weakly dependent upon V, see for example Table 4 of Molinari et al. (2011).

The heat dissipated at the tool chip interface is due to frictional heating. It has been shown that the increasing of temperature $T_{\max} - T_1$ between the entry of the tool rake face and the hot spot could be scaled by a power law with respect to the chip velocity with exponent 0.5: $T_{\max} - T_1 \propto (V_c)^{0.5}$, Fig. 9b.

For all values of V the maximum chip temperature $T_{\max}$ increases with μ, Fig. 6e. The position of the hot spot $x_{\max}$ is nearly insensitive to V, Fig. 13b.

6.2. High friction ($0.4 \leqslant \mu \leqslant 1$)

The situation is totally different for large values of the sliding friction coefficient ($0.4 \leqslant \mu \leqslant 0.8$). An abrupt transition towards a contact dominated by sticking was observed when increasing the cutting speed, see Fig. 17b. For $\mu = 1$ sticking contact is dominant in the whole range of cutting speeds $1\ \mathrm{ms}^{-1} \leqslant V \leqslant 50\ \mathrm{ms}^{-1}$.

When sticking is dominant, the tool–chip interface response is mostly controlled by the average shear flow stress of the work-material, $\bar{\tau}_{SZ}$, along the sticking contact. Then, the effect of the sliding friction coefficient μ is almost wiped out. This is the reason why at large cutting velocities the process variables become weakly dependent on μ. This was verified in Fig. 6e for $T_{\max}$, in Fig. 7a for the shear flow stress $\bar{\tau}_{SZ}$ along the sticking zone, in Fig. 16b and c for the thickness of the secondary shear zone, and in Fig. 17a for the sticking length. This is also true for other process variables reported in Table 4 of Molinari et al. (2011).

For $\mu \geqslant 0.4$ the thickness of the secondary shear zone (induced by sticking) appeared to be inversely proportional to the local chip velocity, see Fig. 16c. At large cutting speeds, the secondary shear zone becomes so thin that it behaves as a boundary layer. Then, the heat dissipated in the secondary shear zone is localized nearby the tool face.

The evolution of process variables observed for increasing cutting velocities is controlled by the thermal softening of $\bar{\tau}_{SZ}$. It was shown that $\bar{\tau}_{SZ}$ is mainly governed by a characteristic interface temperature which was taken as the maximum chip temperature $T_{\max}$, see Fig. 7b. By extrapolating the results of Fig. 7b, $\bar{\tau}_{SZ}$ appeared to vanish when $T_{\max}$ reaches the value T^* larger than (but close to) the melting temperature T_m of the work-material.

At large cutting velocities, the process variables seem to tend to an asymptotic regime. This was the case for instance for the cutting and feed forces, see Fig. 18a of Molinari et al. (2011), for $T_{\max}$ in Fig. 6e and for $\bar{\tau}_{SZ}$ in Fig. 7a.

The laws governing this asymptotic regime will be characterized in the following. For that purpose, we consider the mean friction coefficient $\bar{\mu}$ characterizing the overall tribological response of the tool rake face ($0 \leqslant x \leqslant l_c$), defined as: $\bar{\mu} = \frac{F_t(rake)}{F_n(rake)}$.

By $F_n(rake)$ and $F_t(rake)$ we designate respectively the normal and the tangential components of the force exerted by the chip on the part IJ ($0 \leqslant x \leqslant l_c$) of the tool, see Fig. 2. It was shown by Molinari et al. (2011) that, for $\mu \geqslant 0.4$, the dependence of $\bar{\mu}$ with respect to cutting conditions can be described by a simple phenomenological law of the form:

$$\bar{\mu} = \bar{\mu}(T_{\max}) \tag{22}$$

This result means that the overall friction coefficient of the tool rake face is mostly controlled by the level of the chip temperature at the interface. Thus, $\bar{\mu}$ appears to be affected by the cutting speed V and the uncut chip-thickness t_1 through the sole variable $T_{\max}$ (maximum chip temperature on the rake face).

It was also found that the mean friction coefficient vanishes when $T_{\max}$ reaches the critical temperature T^{**} which is larger than (but close to) T_m.

$$\bar{\mu}(T^{**}) = 0 \tag{23}$$

It was further demonstrated by Molinari et al. (2011) that $\bar{\mu}$ is nearly independent of the value of the sliding friction coefficient μ when $T_{\max}$ is large enough i.e. at high cutting speeds. As a consequence T^{**} can be considered as independent of μ.

To characterize the asymptotic regime at high cutting velocities, Eq. (15) is written as:

$$T_{\max} - T_1 = K_1 \frac{F_n(rake)\bar{\mu}}{\sqrt{\rho C_p k l_c}} \sqrt{V_c} \tag{24}$$

Let us define the limiting value of a given variable Ω at large velocities as:

$$\Omega^{\infty} = \lim_{V \to \infty} \Omega \tag{25}$$

Then, Eq. (24) gives for $V \to \infty$:

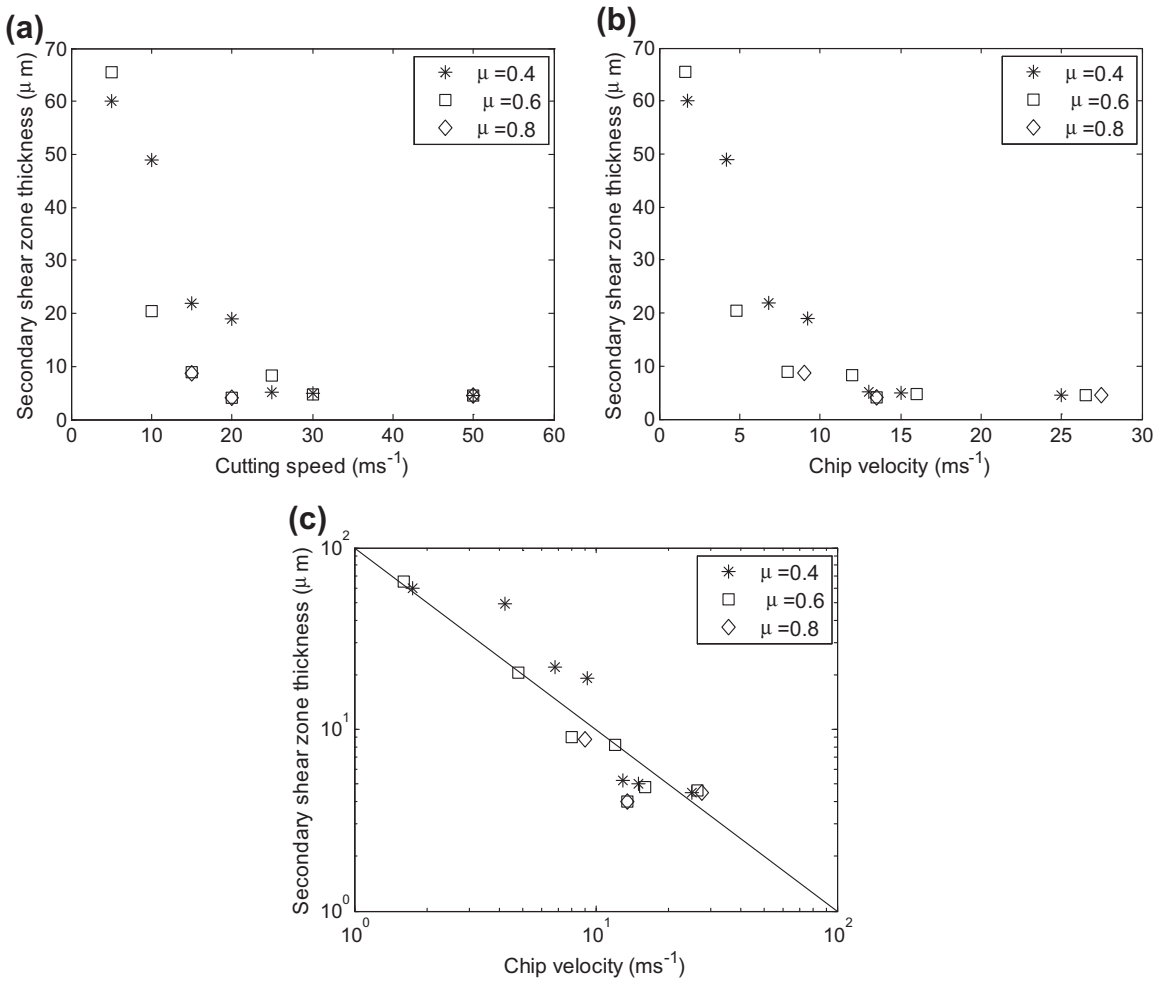

Fig. 16. Thickness of the secondary shear zone l_2, evaluated at the point S of the rake face. Various values of the sliding friction coefficient are considered. The mesh size is about 2 μm. Test conditions T4 of Table 3 are adopted. (a) l_2 versus cutting speed V, (b) l_2 versus the local chip velocity V_c calculated at S′, (c) l_2 versus V_c (loglog diagram). Note that the slope (−1) corresponds to a variation of l_2 as V_c^{-1}, in accordance with theoretical results on adiabatic shearing.

$$T^{\infty}_{\max} - T^{\infty}_{1} = K^{\infty}_{1} \frac{F^{\infty}_{n}(rake)\bar{\mu}^{\infty}}{\sqrt{\rho C_p k l^{\infty}_{c}}} \lim_{V\to\infty} \sqrt{V_c} \tag{26}$$

Since all variables in Eq. (26) have finite limit, except for $\lim_{V\to\infty}\sqrt{V_c}$, we must have $\bar{\mu}^{\infty} = 0$. Thus for large cutting speeds, the mean friction coefficient of the rake face is tending to zero. To have $\bar{\mu}^{\infty} = 0$, the shear stress applied on the rake face has to vanish. This implies that $\bar{\tau}^{\infty}_{SZ} = 0$ and $l^{\infty}_{p} = l^{\infty}_{c}$ (sticking occurs along the whole contact, otherwise we would have a non-zero shear stress along the sliding contact, in contradiction with $\bar{\mu}^{\infty} = 0$). $\bar{\tau}_{SZ}$ vanishes for $T_{\max} = T^{*}$ according to the constitutive law defined above for $\bar{\tau}_{SZ}$. On the other hand, $\bar{\mu}^{\infty} = 0$ implies that $T_{\max} = T^{**}$, according to Eq. (23). Thus, necessarily we have $T^{*} = T^{**}$, i.e. $\bar{\tau}_{SZ}$ and $\bar{\mu}$ have the same critical temperature T^{*} (independent of μ as for T^{**}).

The asymptotic response of the system can be characterized by considering the first order Taylor expansion of $\bar{\mu}(T_{\max})$ at $T_{\max} = T^{*}$:

$$\bar{\mu}(T_{\max}) \approx b(T^{*} - T_{\max}) \quad (\text{for } T_{\max} \text{ close to } T^{*}) \tag{27}$$

We have used the fact that $\bar{\mu}(T^{*}) = 0$ and we have introduced the following definition:

$$b = -\bar{\mu}'(T^{*}) > 0 \tag{28}$$

where $\bar{\mu}'$ designates the derivative of the function $\bar{\mu}$ with respect to the argument.

By using the relationship (B1) of Appendix B between chip and cutting velocities, Eq. (24) can be rewritten as:

$$T_{\max} - T_1 = h(V)\bar{\mu}(T_{\max})\sqrt{V} \tag{29}$$

where $h = K_1 \frac{F_n(rake)}{\sqrt{\rho C_p k l_c}} \sqrt{\frac{\sin\phi}{\cos(\phi-\alpha)}}$.

Introducing (27) into (29) we obtain a linear equation for $T_{\max}$ which can be resolved as:

$$T^{*} - T_{\max} = \frac{T^{*} - T_1}{1 + bh(V)\sqrt{V}} \tag{30}$$

At large values of V, we have:

$$T^{*} - T_{\max} \approx \frac{T^{*} - T_1}{bh^{\infty}} \frac{1}{\sqrt{V}} \tag{31}$$

where h^{∞} is defined according to (25). Substitution of (31) into (27) gives:

$$\bar{\mu} \approx \frac{T^{*} - T_1}{h^{\infty}} \frac{1}{\sqrt{V}} \tag{32}$$

To analyze the asymptotic response, it should be noted that T_1 is weakly sensitive to V for $\mu \geqslant 0.4$, see Fig. 6f. Thus (especially at large cutting speeds) T_1 can be considered as constant in the relationships (30) and (31). Then, it appears from the law (31) that $T_{\max}$ is tending asymptotically to T^{*} as $\frac{1}{\sqrt{V}}$. According to (32) $\bar{\mu}$ is decreasing to zero as $\frac{1}{\sqrt{V}}$.

The loglog diagram of Fig. 18a shows for $\mu = 0.8$ the evolution of $\bar{\mu}$ versus the cutting speed in the range $1 \leqslant V \leqslant 50\ \text{ms}^{-1}$. For

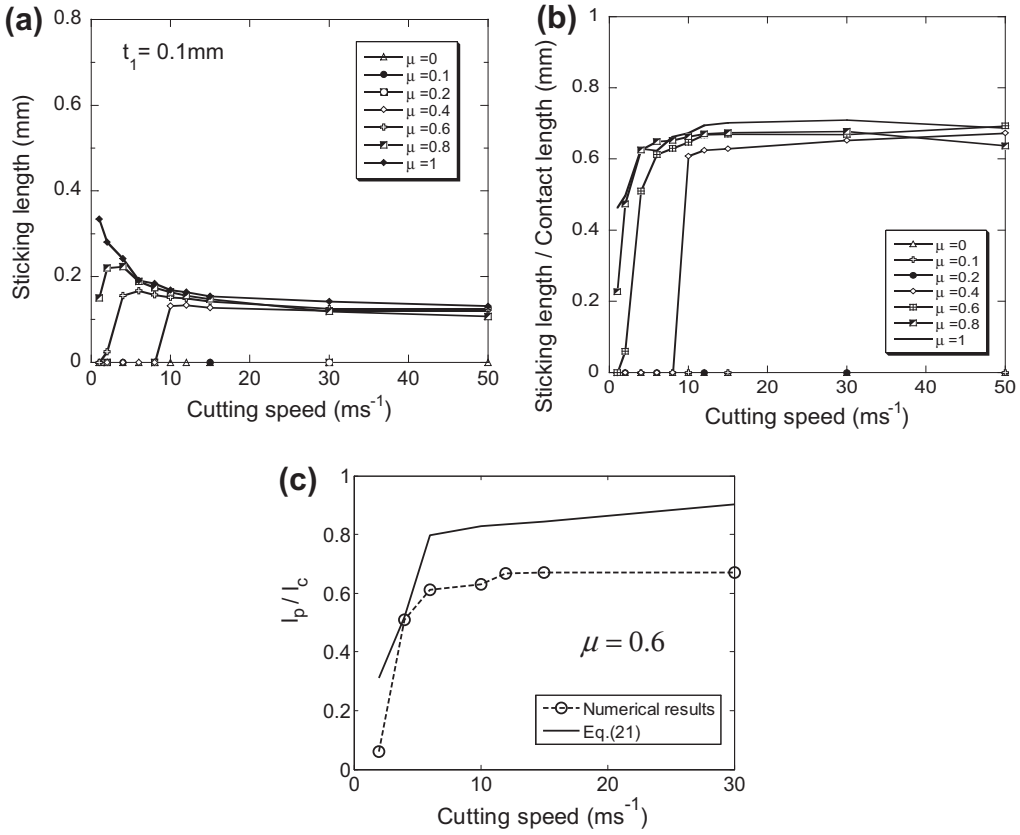

Fig. 17. Sticking contact length l_p in terms of the cutting speed V. Test conditions T4 of Table 3 are adopted. (a) l_p versus V for various values of μ, (b) l_p/l_c versus V for various values of μ, and (c) numerical evaluation of l_p/l_c compared to predictions of Eq. (21) for $\mu = 0.6$.

$4 \leqslant V \leqslant 50$ ms^{-1} the curve has a slope close to -0.4. We have continued this curve by drawing a straight (dashed) line with slope -0.5 according to the law (32) valid at very large velocities. In Fig. 18a no incompatibility in terms of the evolution of the slope is found between numerical results and predictions of Eq. (32) at higher velocities. To report the evolution of $T^* - T_{\max}$ is more difficult since no precise estimate of T^* is available. However, as T^* is close to the melting temperature T_m of the work material, the variation of $T_m - T_{\max}$ in terms of V has been displayed in a loglog diagram, Fig. 18b. A straight line of slope -0.5 has been also drawn. The numerical results show a good correlation with respect to the slope -0.5, in conformity with the law (31).

Naturally, these asymptotic results at large velocities may be sometimes hard to exhibit with experimental tests. Indeed, the hypothesis of continuous chip formation can be in default when increasing the cutting speed due to adiabatic shear banding and other types of damage (cracks, recrystallisation, micro-voiding). However, there are many situations where the asymptotic response reported here is experimentally verified. For the medium carbon steel 42CrMo4 considered in this paper, we refer to the

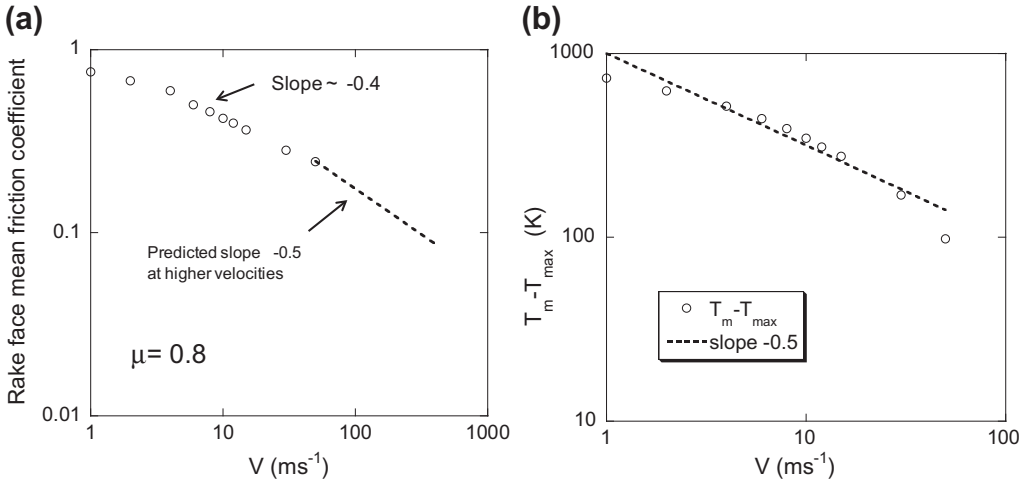

Fig. 18. (a) Evolution of the mean friction coefficient $\bar{\mu}$ versus cutting speed (loglog diagram) for $\mu = 0.8$. Numerical results, represented by circles, are obtained for test conditions T4 of Table 3 in the range $1 \leqslant V \leqslant 50$ ms^{-1}. For $4 \leqslant V \leqslant 50$ ms^{-1} the curve has a slope close to -0.4. This curve has been continued by a straight dashed line with slope -0.5 according to the law (32) valid at very large velocities. (b) Evolution of $T_m - T_{\max}$ in terms of the cutting speed (loglog diagram). T_m is the melting temperature of the work material. Numerical data are indicated by circles. The dashed line displays the slope predicted by Eq. (31).

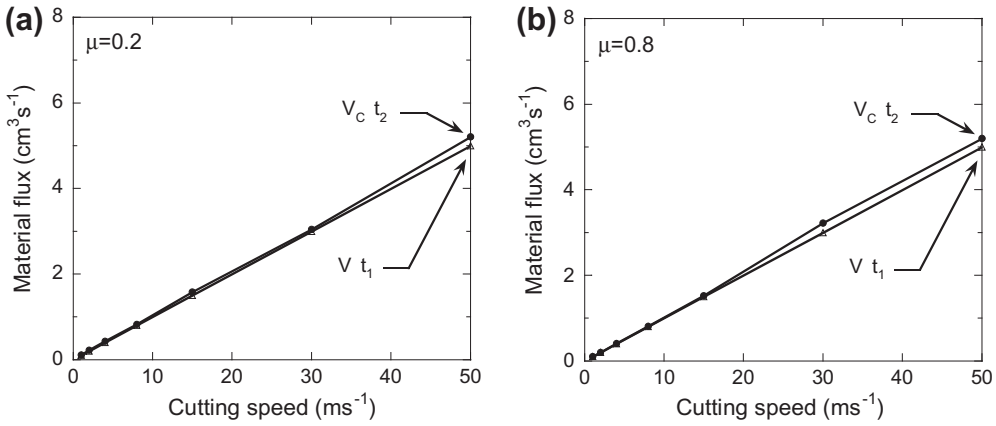

Fig. 19. Volume conservation is illustrated by comparing numerical values of the material flux before and after the primary shear zone in the range of cutting speeds $1 \leqslant V \leqslant 50$ ms^{-1}. Test conditions T4 of Table 3 are adopted. The width of cut is $w = 1$ mm. Two values of the sliding friction coefficient are considered: (a) $\mu = 0.2$ (sliding contact) (b) $\mu = 0.8$ (sticking dominated contact).

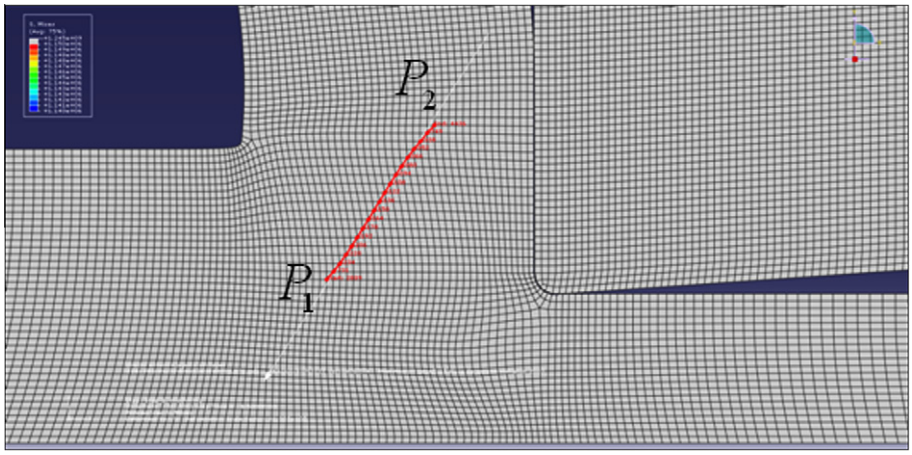

Fig. 20. Path P_1P_2 along which the temperature and the equivalent plastic strain reported in Table 5 are evaluated. The illustration refers to the test (a) of Table 5.

Table 5
Estimates of the shear deformation γ_1 and of the temperature $\hat{T}_1$ at the exit of the primary shear zone. Tests conditions T4 of Table 3 are considered. Results are shown for test (a) ($V = 8$ ms^{-1}, $\mu = 0.2$) and test (b) ($V = 8$ ms^{-1}, $\mu = 0.8$).

Test	Finite Element results			Analytical results	
	ϕ (°)	$\gamma_1^{FE} = \sqrt{3}\varepsilon_{eq}$	$\hat{T}_1^{FE}(K)$	γ_1^{AN} Eq. (C2)	$\hat{T}_1(K)$ Eq. (C1) with γ_1^{FE}
(a)	26.1	2.16	613	2.53	595
(b)	21.3	2.42	645	2.95	634

experimental data reported in Fig. 2 of Molinari et al. (2011) which show, for the cutting and thrust forces and the apparent friction coefficient, asymptotic evolutions at large cutting speeds similar to those predicted by the present numerical model.

7. Conclusions

Understanding the nature of contact at the tool–chip interface is essential for the modeling of cutting processes. The aim of the present work was to develop the fundamental knowledge on contact regimes under the extreme conditions encountered in machining, having in mind that this understanding can be useful to other situations where severe contact conditions are involved as in impact and penetration mechanics.

Tool–chip contact in orthogonal cutting was investigated with Finite Element simulations and analytical formulations. A Coulomb friction law with constant sliding friction coefficient (i.e. independent from cutting conditions) was considered.

It was shown that the chip temperature controls the nature of the tool–chip contact (sliding versus sticking) by tuning the level of the flow stress of the work-material (thermal softening). An increasing of temperature leads to a decay of the flow stress that favors sticking contact. With this in mind, much effort was devoted to characterize the chip temperature at the rake face and to determine the influence of cutting conditions on temperature and nature of contact. We focused on the roles of cutting speed and feed. The rake angle was fixed to zero. For a large range of cutting speeds, feed rates and values of the sliding friction coefficient μ, the following points were established:

- Sticking contact is promoted by high friction, and, because of chip heating, by high cutting speed and large feed.
- For large friction ($\mu \geqslant 0.4$) a brutal transition to a contact dominated by sticking is observed when increasing the cutting speed.

- The increasing of the chip temperature along the rake face was identified by analytical means in terms of Péclet number and mean shear stress along the interface.
- The increase of temperature along the interface was characterized by a power-law dependence with respect to the chip velocity with an exponent depending of the nature of contact. For high values of the sliding friction coefficient, contact is dominated by sticking and the exponent has low value (0.2). Then, the chip temperature shows strong velocity dependence at low cutting speeds and weak dependence at high cutting speeds. For small values of the sliding friction coefficient, the contact is dominated by sliding and the exponent in the power law has larger value (0.5).
- When contact is dominated by sticking (this excludes very small sliding friction coefficients), the chip interface temperature can be related to the cutting speed V and the feed t_1 through the dimensionless number Vt_1/a (where a is the thermal diffusivity of the work-material). This number appears as an essential parameter controlling the cutting process.
- The morphology of the secondary shear zone (sticking contact) was characterized by sticking length and thickness. The thickness was found to be inversely proportional to the local chip velocity in the range of cutting velocities considered ($1\ \mathrm{ms}^{-1} \leqslant V \leqslant 50\ \mathrm{ms}^{-1}$). At high cutting speeds, the secondary shear zone takes the appearance of a boundary layer with a thickness of few micro-meters.
- When contact is dominated by sticking, the system is governed by an asymptotic regime at high cutting speeds. This asymptotic response is related to the existence of a boundary layer regime (along the sticking zone) and to the increase of the chip temperature at the rake-face towards the melting temperature. Asymptotic laws governing the evolution of the chip temperature and of the mean friction coefficient with respect to the cutting speed were theoretically derived.

Despite the simplicity of the contact model based on the Coulomb friction law, reasonable agreements were found with experimental trends. All along the paper, the interplay between analytic and numerical approaches allowed for checking the consistency of numerical simulations, making the interpretation of data more meaningful and offering a route for subsequent improvements of analytical models of machining.

Acknowledgments

A.M. acknowledges the support of Carlos III University with a Catedra de Excelencia funded by Banco Santander. Fruitful discussions with Prof. Ramón Zaera are also acknowledged by the authors.

Appendix A. Plastic flow analysis along the sticking zone

It is demonstrated that the plastic flow along the sticking zone is identical to simple shearing in the direction x (Fig. 2) if and only if the following condition is satisfied for $0 \leqslant x \leqslant l_p$:

$$\tau = \frac{\sigma_{eq}}{\sqrt{3}} \tag{A1}$$

$\tau = s_{xy} = s_{yx}$ is the shear stress at the tool–chip interface.

Firstly, let us assume that we have simple shearing in the direction x. Then, all the components of the plastic strain rate tensor are equal to zero except for $d^p_{xy} = d^p_{yx}$. From the J_2-flow law, we have $\underline{d}^p = \lambda \underline{s}$. Therefore $s_{xy} = s_{yx}$ are the sole non-zero components of the deviatoric stress $\underline{s}$. Consequently, the Mises- equivalent stress σ_{eq} is related to the shear stress τ by (A1).

Conversely, let us assume that the plastic flow is not identical to simple shearing along the tool rake-face. Thus, there exists a component d^p_{ij} different from zero and different from d^p_{xy}. Due to the J_2-flow law it results immediately that $\sigma_{eq} > \sqrt{3}\tau$ and (A1) is violated.

Appendix B. Consistency of the velocity field with the conservation of volume by plastic deformation.

Consider the segment KK' in Fig. 2 drawn perpendicularly to the tool rake face. The point K is defined such that the tangent at K to the chip surface is parallel to the tool rake-face. The chip thickness is defined as $t_2 = KK'$. Along KK' the particle velocity $\underline{\hat{V}}$ is non-uniform. The component $\hat{V}_x$ parallel to the rake face is almost an affine function of the distance y to the tool and is increasing with y. Thus, the material flux across the line KK' is given by $q_2 = t_2 V_c$, where $V_c = \frac{\hat{V}_x(K) + \hat{V}_x(K')}{2}$ characterizes the chip velocity. On the other hand, the flux of work material flowing toward the tool is $q_1 = t_1 V$, where V is the cutting speed and t_1 is the uncut chip thickness. Since plastic flow is volume preserving we should have (by neglecting elastic deformation) $q_1 = q_2$. The results of Fig. 19 reported for a width of cut of $w = 1$ mm and for $\mu = 0.2$ and $\mu = 0.8$ show that this relationship is well satisfied.

As a consequence, a simple way of evaluating the average chip velocity on KK' will be to employ the usual relationship derived from volume conservation:

$$V_c^{theor} = V \frac{\sin\phi}{\cos(\phi - \alpha)} \tag{B1}$$

Appendix C. Calculation of the temperature at the exit of the primary shear zone

Tests conditions reported in T4 of Table 3 are considered. Table 5 shows for the test (a) ($V = 8\ \mathrm{ms}^{-1}$, $\mu = 0.2$) and test (b) ($V = 8\ \mathrm{ms}^{-1}$, $\mu = 0.8$) Finite Element method estimates of the temperature $\hat{T}_1$ and of the plastic shear deformation γ_1 undergone by a material element after crossing the primary shear zone. $\hat{T}_1$ is the (nodal) temperature at the exit of the primary shear zone obtained by following a path as indicated in Fig. 20. γ_1 is estimated in terms of the equivalent Mises plastic strain ε_{eq} as: $\gamma_1^{FE} = \sqrt{3}\varepsilon_{eq}$.

The temperature $\hat{T}_1$ at the exit of the primary shear zone (PZ) can be evaluated by analytical means in terms of the mean shear flow stress $\bar{\tau}_{PZ}$ and of the plastic shear deformation γ_1. Assuming that heat transfer effects are negligible (adiabatic process), the temperature rise between the entry and the exit of the primary shear zone is given by the energy equation:

$$(\Delta T)_{PZ} = \frac{\beta \bar{\tau}_{PZ} \gamma_1}{\rho C_p} \tag{C1}$$

Note that $\bar{\tau}_{PZ}$ is weakly sensitive to cutting conditions and to the value of μ, see results reported in Molinari et al. (2011), and is about $\bar{\tau}_{PZ} = 640$ MPa. $\hat{T}_1 = 273\ \mathrm{K} + (\Delta T)_{PZ}$ is evaluated in the last column of Table 5 by using (C1) with $\beta = 0.9$ and the above values of $\bar{\tau}_{PZ}$ and γ_1^{FE}. A good agreement is found in Table 5 with respect to $\hat{T}_1^{FE}$ directly obtained from FE calculations. This is an indication that the following hypotheses upon which Eq. (C1) is based are well satisfied: (i) the plastic deformation mode in the PZ is simple shearing and (ii) the deformation process is adiabatic.

In Table 5, the shear deformation across the primary shear zone has been also calculated by using the usual expression (with $\alpha = 0$):

$$\gamma_1^{AN} = \frac{\cos(\alpha)}{\sin(\phi)\cos(\phi - \alpha)} \tag{C2}$$

The shear angle $\phi = \arctan(t_1/t_2)$ is given in Table 4 of Molinari et al. (2011). Results obtained with Eq. (C2) correlate reasonably with γ_1^{FE} with a slight overestimation. The temperature $\hat{T}_1$ obtained with (C1) and (C2) would be also slightly overestimated ($\hat{T}_1 = 651$ K for test (a) and $\hat{T}_1 = 709$ K for test (b)).

Appendix D. Characterization of stress softening along the sticking zone

Test (b) of Appendix C is considered here ($\mu = 0.8$, $V = 8$ m/s, $t_1 = 0.1$ mm, $R = 0.015$ mm, $\kappa = 2000\,\mathrm{W\,m^{-2}\,K^{-1}}$). The superscripts *1* and *2* refer respectively to the entry ($x = 0$) and the exit ($x = l_p$) of the sticking zone. At these points of the rake face, values of the Mises equivalent stress, temperatures, cumulated plastic strain are given by: $\frac{\sigma_{eq}^{(1)}}{\sqrt{3}} = 509$ MPa, $T_1^{(1)} = 1010$ K, $\varepsilon_{eq}^{(1)} = 9.07$ and $\frac{\sigma_{eq}^{(2)}}{\sqrt{3}} = 319$ MPa, $T_1^{(2)} = 1402$ K, $\varepsilon_{eq}^{(2)} = 21.8$. The stress drop can be characterized by the ratio:. $\frac{\sigma_{\mathrm{eq}}^{(2)}}{\sigma_{\mathrm{eq}}^{(1)}} = \frac{f(\varepsilon_{eq}^{(2)})g(\dot{\varepsilon}_{eq}^{(2)})h(T_1^{(2)})}{f(\varepsilon_{eq}^{(1)})g(\dot{\varepsilon}_{eq}^{(1)})h(T_1^{(1)})} = 0.63$.

The respective contributions of thermal softening and of strain hardening can be evaluated since temperature and equivalent plastic strains are known: $\frac{h(T_1^{(2)})}{h(T_1^{(1)})} = 0.541$ and $\frac{f(\varepsilon_{eq}^{(2)})}{f(\varepsilon_{eq}^{(1)})} = 1.070$. The functions $h(\cdot)$ and $f(\cdot)$ are obtained from the Johnson–Cook law. From the value of the stress ratio, the contribution of the rate dependence can be estimated as $\frac{g(\dot{\varepsilon}_{eq}^{(2)})}{g(\dot{\varepsilon}_{eq}^{(1)})} = 1.08$. Thus, it can be concluded that the variation of the shear stress along the sticking zone is mostly due to thermal softening of the work material (factor 0.541) with second order stiffening effects of strain hardening (factor 1.07) and rate sensitivity (factor 1.08).

References

Abaqus Manual, 2003. Version 6.4, Hibbit. Karlsson & Sorenson Inc., Providence, USA.

Adibi-Sedeh, A.H., Madhavan, V., 2003. Understanding of finite element analysis results under the framework of Oxley's machining model. In: Proceedings of the Sixth CIRP International Workshop on Modeling of Machining Operations, Hamilton, Canada.

Arrazola, P.J., Ugarte, D., Domínguez, X., 2008. A new approach for the friction identification during machining through the use of finite element modeling. Int. J. Mach. Tools Manuf. 48 (2), 173–183.

Arrazola, P.J., Özel, T., 2010. Investigation on the effects of friction modeling in finite element simulation of machining. Int. J. Mech. Sci. 52, 31–42.

Bahi, S., Nouari, M., Moufki, A., ElMansori, M., Molinari, A., 2011. A new friction law for sticking and sliding contacts in machining. Tribol. Int. 44, 764–771.

Bai, Y., Dodd, B., 1992. Adiabatic Shear Localization: Occurrence, Theories and Applications. Pergamon.

Bonnet-Lebouvier, A.S., Molinari, A., Lipinski, P., 2002. Analysis of the dynamic propagation of adiabatic shear bands. Int. J. Solids Struct. 39, 4249–4269.

Brocail, J., Watremez, M., Dubar, L., 2010. Identification of a friction model for modelling of orthogonal cutting. Int. J. Mach. Tools Manuf. 50, 807–814.

Childs, T.H.C., Mahdi, M.I., Barrow, G., 1989. CIRP Annals Manufacturing Technology, pp. 55–58.

Childs, T.H.C., Dirikolu, M.H., Maekawa, K., 1998. Modelling of friction in the simulation of metal machining. 24th Leeds–Lyon Symposium on Tribology. Tribology Series, vol. 34. Elsevier, Amsterdam, pp. 337–346.

Childs, T.H.C., 2006a. Numerical experiments on the influence of material and other variables on plane strain continuous chip formation in metal machining. Int. J. Mech. Sci. 48 (3), 307–322.

Childs, T.H.C., 2006b. Friction modelling in metal cutting. Wear 260 (3), 310–318.

Dinzart, F., Molinari, A., 1998. Structure of adiabatic shear bands in thermo-viscoplastic materials. Eur. J. Mech. A/Solids 17, 923–938.

Dirikolu, M.H., Childs, T.H.C., Maekawa, K., 2001. Finite element simulation of chip flow in metal machining. Int. J. Mech. Sci. 43, 2699–2713.

Filice, L., Micari, F., Rizzuti, S., Umbrello, D., 2007. A critical analysis on the friction modelling in orthogonal machining. Int. J. Mach. Tools Manuf. 47 (3–4), 709–714.

Gioia, G., Ortiz, M., 1996. The two-dimensional structure of dynamic boundary layers and shear bands in thermoviscoplastic solids. J. Mech. Phys. Solids 44, 251–292.

Guillot, E., Bourouga, B., Garnier, B., Brocail, J., 2008. Measurement of the thermal contact parameters at a workpiece-tool interface in a HSM process. In: Proceedings Esaform Congress, Lyon.

Haglund, A.J., Kishawy, H.A., Rogers, R.J., 2005. On friction modeling in orthogonal machining: an arbitrary Lagrangian–Eulerian finite element model. Trans. NAMRI/SME 33, 589–596.

Kountanya, R., Al-Zkeri, I., Altan, T., 2009. Effect of tool geometry and cutting conditions on experimental and simulated chip morphology in orthogonal hard turning of 100Cr6 steel. J. Mater. Process. Technol. 209, 5068–5076.

Marusich, T.D., Ortiz, M., 1995. Modeling and simulation of high-speed machining. Int. J. Numer. Methods Eng. 38, 3675–3694.

Molinari, A., Clifton, R., 1983. Localization of the viscoplastic deformation in simple shear: exact results in the non-linear theory. CR Acad. Sci. Paris II 296, 1–4.

Molinari, A., Moufki, A., Dudzinski, D., 1997. Analysis of the Behaviour of 42CrMo4 Steel. Final Technical Report, Université de Metz-CREAS Ascometal.

Molinari, A., Musquar, C., Sutter, G., 2002. Adiabatic shear banding in high speed machining of Ti–6Al–4V: experiments and modeling. Int. J. Plasticity 18, 443–459.

Molinari, A., Ravichandran, G., 2006. Modeling plastic shocks in periodic laminates with gradient plasticity theories. J. Mech. Phys. Solids 54, 2495–2526.

Molinari, A., Cheriguene, R., Miguelez, H., 2011. Numerical and analytical modelling of orthogonal cutting: the link between local variables and global contact characteristics. Int. J. Mech. Sci. 53, 183–206.

Moufki, A., Molinari, A., Dudzinski, D., 1998. Modelling of orthogonal cutting with a temperature dependent friction law. J. Mech. Phys. Solids 46 (10), 2103–2138.

Movahhedy, M.R., Gadala, M.S., Altintas, Y., 2000. FE modeling of chip formation in orthogonal metal cutting process: an ALE approach. Mach. Sci. Technol. 4, 15–47.

Movahhedy, M.R., Altintas, Y., Gadala, M.S., 2002. Numerical analysis of metal cutting with chamfered and blunt tools. ASME J. Manuf. Sci. Eng. 124, 178–188.

Olovsson, L., Nilsson, L., Simonsson, K., 1999. An ALE formulation for the solution of two-dimensional metal cutting problems. Comput. Struct. 72, 497–507.

Özel, T., Zeren, E., 2005. Finite element method simulation of machining of AISI 1045 steel with a round edge cutting tool. In: Proceedings of the Eighth CIRP International Workshop on Modeling of Machining Operations, Chemnitz, Germany, April 10–11, pp. 533–542.

Özel, T., 2006. Influence of friction models on finite element simulations of machining. Int. J. Mach. Tool Manuf. 46 (5), 518–530.

Ozlu, E., Molinari, A., Budak, E., 2010. Two-zone analytical contact model applied to orthogonal cutting. Mach. Sci. Technol. 14, 323–343.

Rakotomalala, R., Joyot, P., Touratier, M., 1993. Arbitrary Lagrangian–Eulerian thermo- mechanical finite element model of material cutting. Commun. Numer. Methods Eng. 9, 975–987.

Recht, R.F., 1964. Catastrophic thermoplastic shear. J. Appl. Mech. 86, 189–193.

Rittel, D., Ravichandran, G., Venkert, A., 2006. The mechanical response of pure iron at high strain rates under dominant shear. Mater. Sci. Eng. A 432, 191–201.

Shirakashi, T., Usui, E., 1976. Simulation analysis of orthogonal metal cutting process. J. Jpn. Soc. Prec. Eng. 42 (5), 340–345.

Sutter, G., Molinari, A., Faure, L., Klepaczko, J.R., Dudzinski, D., 1998. An experimental study of high speed orthogonal cutting. ASME J. Manuf. Sci. Eng. 120, 169–172.

Sutter, G., Faure, L., Molinari, A., Ranc, N., Pina, V., 2003. An experimental technique for the measurement of temperature fields for the orthogonal cutting in high speed machining. Int. J. Mach. Tools Manuf. 43, 671–678.

Sutter, G., Molinari, A., 2005. Analysis of the cutting force components and friction in high speed machining. J. Manuf. Sci. Eng. 127, 245–250.

Sutter, G., Ranc, N., 2007. Temperature fields in a chip during high-speed orthogonal cutting – an experimental investigation. Int. J. Mach. Tools Manuf. 47, 1507–1517.

Tresca, H., 1878. On further applications of the flow of solids. Proc. Inst. Mech. Engrs. 30, 301.

Wright, T.W., Ockendon, H., 1992. A model for fully-formed shear bands. J. Mech. Phys. Solids 40, 1217–1226.

Wright, T.W., 2002. The Physics and Mathematics of Adiabatic Shear Bands. Cambridge University Press.

Zener, C., Hollomon, J.H., 1944. Effect of strain rate upon plastic flow of steel. J. Appl. Phys. 15, 22–32.

Zorev, N.N., 1963. Inter-relationship between shear processes occurring along tool face and shear plane in metal cutting. In: International Research in Production Engineering. ASME, New York, pp. 42–49 .